

# Re-analysis of data on $a_0(1450)$ and $a_0(980)$

D.V. Bugg<sup>1</sup>,

Queen Mary, University of London, London E1 4NS, UK

## Abstract

Four sets of data determining parameters of  $a_0(1450)$  and  $a_0(980)$  are re-analysed. These are Crystal Barrel data for  $\bar{p}p$  annihilation at rest to  $\eta\pi^0\pi^0$  in (i) liquid hydrogen and (ii) gas, and to (iii)  $K_L^0\pi^\pm K^\mp$  and (iv)  $\omega\pi^+\pi^-\pi^0$  (mostly  $\omega\rho\pi$ ). Dispersive corrections due to opening of inelastic thresholds are treated fully. This stabilises parameters of  $a_0(1450)$  substantially. The mass of its peak is  $1448 \pm 13(stat) \pm 25(syst)$  MeV and its mean full width at half maximum is  $192 \pm 9 \pm 9$  MeV. The pole position is  $M - i\Gamma/2 = 1432 \pm 13 \pm 25 - i(98 \pm 5 \pm 5)$  MeV. At the peak,  $\eta\pi$ ,  $\omega\rho$  and  $a_0(980)\sigma$  decay intensities are in the ratios  $1 : 9.2 \pm 0.8 \pm 1.3 : 3.1 \pm 0.2 \pm 0.9$ . There is no evidence for a separate  $a_0$  near 1300 MeV claimed by Obelix. Parameters of  $a_0(980)$  are updated to  $M = 987.4 \pm 1.0 \pm 3.0$  MeV,  $g^2(\eta\pi) = 0.164 \pm 0.007 \pm 0.010$  GeV<sup>2</sup>,  $g^2(KK)/g^2(\eta\pi) = 1.05 \pm 0.07 \pm 0.05$ . Its dominant second sheet pole in the  $KK$  channel is at  $(989 \pm 1 \pm 5) - i(40 \pm 2 \pm 4)$  MeV. Finally, the nature of the prominent  $J^{PC} = 0^{-+} \rightarrow \omega\rho$  signal in  $\omega\rho\pi$  data is also clarified.

PACS: 13.25.Gv, 14.40.Gx, 13.40.Hq

## 1 Introduction

The main objective of this work is to re-examine the parameters of  $a_0(1450)$ . It appears in the summary table of the Particle Data Group [1] although it has been observed decisively in only one set of data, from Crystal Barrel on  $\bar{p}p \rightarrow \eta\pi^0\pi^0$  at rest [2], [3], [4], [5]. There is further evidence from other data of the same experiment. It has been confirmed in the  $\omega\rho$  channel in  $\omega\pi^+\pi^-\pi^0$  data at rest [6]. Its  $KK$  decays are observed in  $(K_L^0 K^\pm)\pi^\mp$  data at rest [7]. There is also evidence for it in  $\bar{p}p \rightarrow (\eta'\pi^0)\pi^0$  [8] and  $\bar{p}p \rightarrow (\eta\pi^+\pi^-\pi^\pm)\pi^\mp$  [9] at rest.

Its branching ratio to  $\omega\rho$  in Ref. [6] is a factor  $\sim 11$  larger than to  $\eta\pi$  (and will be revised here slightly). The fact that its branching ratio to  $\eta\pi$  is  $< 10\%$  explains why  $a_0(1450)$  has been elusive in data for  $\pi^-p \rightarrow \pi\pi n$ . An important point is that the phase space for the  $\omega\rho$  channel has a rapid  $s$ -dependence, so it is inappropriate to fit the  $a_0(1450)$  with a Breit-Wigner amplitude of constant width, as was done in the early work. Its line-shape and the relation between magnitude and phase are affected strongly by dispersive effects, which are treated fully here. Attention to this detail improves considerably the stability of fitted parameters and makes the signal in both  $\eta\pi$  and  $\omega\rho$  much clearer.

The  $a_0(980)$  is examined along the same lines. The dispersive effect due to the opening of the  $KK$  channel plays a critical role and again improves the quality of the fit to  $\eta\pi^0\pi^0$  data. Adler zeros are included into its  $\eta\pi$  and  $\eta'\pi$  decay channels. For these reasons, its parameters change significantly from earlier work.

The dispersive effects may be unfamiliar to experimentalists, though well known to theorists since the 1950's. Experimental analyses have conventionally been done with a Breit-Wigner amplitude with denominator

$$D(s) = M^2 - s - i \sum_j g_j^2 \rho_j(s). \quad (1)$$

Here  $\rho_j(s)$  is the phase space for each decay channel  $j$  as a function of invariant mass squared  $s$ , possibly including a form factor. The  $g_j$  are coupling constants to each decay amplitude. Let us write

$$D(s) = M^2 - s - \sum_j \Pi_j(s) \quad (2)$$

with  $\text{Im } \Pi_j(s) = g_j^2 \rho_j(s)$ . Because scattering amplitudes are analytic functions, any  $s$ -dependence of  $\text{Im } \Pi_j(s)$  necessarily leads to a term in  $D(s)$  given by

$$\text{Re } \Pi_j(s) = \frac{1}{\pi} \text{P} \int_{s_{\text{thr}}}^{\infty} \frac{\text{Im}_j(s') ds'}{s' - s}. \quad (3)$$

Here P denotes the Principal Value Integral and  $s_{\text{thr}}$  is the value of  $s$  at threshold. This is known as a dispersive contribution. It is equivalent to evaluating loop diagrams. If  $\rho(s)$  changes rapidly, as it does at the opening of

---

<sup>1</sup>email address: D.Bugg@rl.ac.uk

a sharp threshold, the dispersive term becomes dominant and affects the parameters of the resonance strongly. Fig. 1 below illustrates the result for  $a_0(980)$ . There is a prominent cusp in  $\text{Re } \Pi_{KK}(s)$ , centred at the threshold. It plays a major role in locking the resonance to this threshold [10]. One objective of the present work is to refine the parameters of  $a_0(980)$  to include this effect.

Consider next  $a_0(1450)$ . The  $\omega\rho$  threshold is quite sharp and has a large effect on the line-shape near 1450 MeV. There is a cusp at the  $\omega\rho$  threshold which also acts as an attractor. This may be the reason that  $a_0(1450)$  is higher in mass than  $f_0(1370)$  and  $K_0(1430)$ .

Section 2 reviews dispersive effects. In principle they apply to all resonances. Fortunately, resonances with broad thresholds may be approximated by the pole term alone and this will be demonstrated here for  $a_2(1320)$ . There may be small residual effects far from resonance, but in practice these effects are tolerable at present.

Section 3 discusses fits to  $\eta\pi^0\pi^0$  and  $\omega\pi^+\pi^-\pi^0$  data, hence parameters of  $a_0(1450)$ . In the present work, the widths of  $a_0(1450)$  to  $KK$  and  $\eta\pi$  are small, so there is no longer significant overlap between these two resonances and therefore little correlation between their parameters. An incidental feature of the re-analysis of  $\omega\pi^+\pi^-\pi^0$  data is an improved understanding of the large  $J^{PC} = 0^{-+} \omega\rho$  signal observed there.

Section 4 gives results for  $a_0(980)$  and Section 5 discusses  $KK$  coupling of  $a_0(1450)$  and parameters of  $a_0(980)$ . The data on  $K_L^0 K^\pm \pi^\mp$  do not give an accurate determination of their coupling to  $KK$ , but agree within sizable errors with the better determination from  $\eta\pi^0\pi^0$  data. Section 6 summarises conclusions and makes some remarks on further desirable work.

## 2 Technicalities of the dispersive terms

As an introduction, let us consider  $a_0(980) \rightarrow KK$ . Mass differences between  $K^+K^-$ ,  $K_L^0 K^\pm$  and  $K^0 \bar{K}^0$  will be ignored here because their separations are smaller than mass resolution in data to be fitted. There is a further reason. The VES group has very recently presented data showing that the  $f_1(1285)$  decays to  $3\pi$  [11]. This violates isospin conservation and may well arise from mixing between  $a_0(980)$  and  $f_0(980)$  due to mass differences in the  $KK$  thresholds. Consideration of this problem requires a combined analysis with data on  $f_0(980)$ . It is necessary to take one step at a time and defer this for the present, though one should bear in mind there may be some small effect on parameters fitted to  $a_0(980)$ .

Ignoring mass differences,  $\rho_{KK} = \sqrt{1 - 4m_K^2/s}$ , where  $m_K$  is the mean kaon mass, 495.663 MeV. As  $s \rightarrow \infty$ , the phase space factor  $\rightarrow 1$ . Without any form factor, the dispersion integral of Eq. (3) diverges. Therefore a form factor

$$F_{KK} = \exp(-\alpha k^2) \quad (4)$$

is used to multiply  $g_{KK}$ . Here  $k$  is the momentum of each kaon in the  $KK$  rest frame. This well known form factor assumes a Gaussian source with RMS radius  $R$  given by  $\alpha = R^2/6$ . It turns out that the same value of  $\alpha$  succeeds in fitting all resonances and avoids a multiplicity of parameters. It optimises at  $\alpha = (2.0 \pm 0.25) (\text{GeV}/c)^{-2}$ , corresponding to  $R = 0.68 \pm 0.04$  fm.

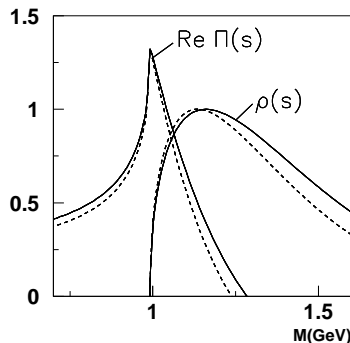


Figure 1:  $KK$  phase space  $\rho'(s)$ , normalised to 1 at its peak and  $\text{Re } \Pi(s)$  (full curves). Dashed curves show results for  $\alpha = 2.5 (\text{GeV}/c)^{-2}$ .

Library subroutines are available for evaluating the Principal Value Integral. Results are shown in Fig. 1 for the product  $\rho' = \rho_{KK}(s)F_{KK}^2(s)$  and for  $\text{Re } \Pi(s)$ . For display purposes, the normalisation is chosen so that  $\rho'$

including the form factor peaks at 1. There is a large cusp in the real part, somewhat larger than the peak of  $\rho'$ . The dashed curves show results with  $\alpha = 2.5 \text{ (GeV/c)}^{-2}$ . In the mass range where the  $a_0(980)$  is strong, the sensitivity to  $\alpha$  is quite small; it comes into play only in the wings of the resonance, where other resonances may mask its effects.

There are two practical points concerning  $\text{Re } \Pi(s)$ . Although it is responsible for attracting  $a_0(980)$  to the  $KK$  threshold, it is convenient to make a subtraction in the Breit-Wigner denominator on resonance:

$$D(s) = M^2 - s - \sum_j \text{Re} [\Pi_j(s) - \Pi_j(M^2)] - i g_j^2 \rho'(s). \quad (5)$$

Secondly, it is convenient to evaluate the dispersion integral as a 2-dimensional array against  $s$  and  $\alpha$ . A simple sub-routine interpolates in this table. When fitting data, one can then optimise  $\alpha$ ,  $M^2$  and  $g^2$  with a standard optimisation program such as Minuit. The dispersive term is proportional to  $g^2$ . Just below the  $KK$  threshold, it varies as  $g_{KK}^2(4m_K^2 - s)/s$  (see algebra in Ref. [10], Eq. 15). This resembles the term  $(M^2 - s)$  in  $D(s)$ . Consequently  $M$  and  $g^2$  become strongly correlated unless there are data determining  $g^2$  separately for every channel.

Because of the correlations, the convergence of the fit is rather poorer than for a simple Breit-Wigner resonance of constant width but still adequate. It is in fact better to let the programme optimise the parameters. The alternative, a grid search over  $M$  and  $g^2$ , is subject to the correlations between them. Standard optimisation programmes work with eigenvectors and circumvent the correlations.

A general point is that all resonances are subject to opening thresholds, hence dispersive effects. However, it fortunately turns out that for broad thresholds the net effect of the dispersive terms becomes small within one full width of the pole. The data can then be parametrised directly in terms of the pole term  $\propto 1/(s - s_{\text{pole}})$ . This conclusion emerged from work on  $f_0(1370) \rightarrow \sigma\sigma$  and  $\rho\rho$  thresholds [12]. For broad thresholds, the dispersive terms have significant effects only far from the pole, and may not be trustworthy there because of uncertainties in form factors. In the present work, thresholds for  $a_1(1260) \rightarrow (\rho\pi)_{L=1}$ ,  $a_2(1320) \rightarrow (\rho\pi)_{L=2}$ ,  $(\eta\pi)_{L=2}$  and  $(KK)_{L=2}$  have been treated fully using the dispersive term. These thresholds open fairly gently because of the centrifugal barriers for orbital angular momentum  $L$  in the decays. The conclusion is the same as in [12]: the line-shapes of these resonances are affected rather little except for their tails.

However, in fitting  $\omega\rho\pi$  data, the rather sharp  $\omega\rho$  threshold does affect the fitted resonances quite strongly. The cusp at the  $\omega\rho$  threshold is broadened by the line-shape of the  $\rho$ . This line-shape may be included in the evaluation of  $\omega\rho$  phase space, then the dispersive effect can be evaluated from the phase space. Suppose as an example  $a_0(1450) \rightarrow \omega\rho$ , followed by  $\rho \rightarrow \pi\pi$ . The 3-body phase space for  $\omega\rho$  is given by the integral

$$\rho'_{\omega\rho}(s) = \int_{4m_\pi^2}^{(\sqrt{s}-m_\omega)^2} \frac{ds_1}{\pi} \frac{4|k||k_1|}{\sqrt{ss_1}} |T_\rho(s_1)|^2 \exp(-2\alpha k^2), \quad (6)$$

where  $T$  is the Breit-Wigner amplitude for the  $\rho$ . Also  $s$  refers to the  $a_0(1450)$  and  $k$  to the momentum of the  $\omega$  or  $\rho$  in the  $a_0$  rest frame;  $s_1$  and  $k_1$  refer to the  $\rho$  and the momenta of the pions in its rest frame. When there is angular momentum in the decay to  $\rho\omega$ , a centrifugal barrier needs to be included.

### 3 Fits to $\bar{p}p \rightarrow \eta\pi^0\pi^0$ and $\omega\pi^+\pi^-\pi^0$

The  $a_0(1450)$  was discovered in Crystal Barrel data for  $\bar{p}p \rightarrow \eta\pi^0\pi^0$  at rest [2], [3], [4], [5]. It also appears in the  $\omega\rho$  channel in  $\omega\rho\pi$  data at rest [6], and in the  $KK$  channel in  $K_L^0 K^\pm \pi^\mp$  data at rest [7]. The latter will be discussed in Section 5, but it turns out that the systematic error in its coupling to  $KK$  is rather large. Its  $KK$  coupling is consistent with the SU(3) prediction, and will be fixed to that value. The same applies to the  $\eta'\pi$  coupling. An analysis of data on  $\bar{p}p \rightarrow \eta'\pi^0\pi^0$  at rest gave results consistent with this prediction [8]. The effects of both  $KK$  and  $\eta'\pi$  channels on the line-shape of  $a_0(1450)$  are similar to  $\eta\pi$  and quite small.

A preliminary comment is required on the fit to data for  $\bar{p}p \rightarrow \omega\pi^+\pi^-\pi^0$ , discussed in sub-section 3.9. The earlier publication did include dispersive effects. The fit to these data changes rather little in the combined fit with  $\eta\pi^0\pi^0$  data. The main improvement to parameters of  $a_0(1450)$  comes from the  $\eta\pi^0\pi^0$  data.

The decays of consequence for the line-shape are  $\eta\pi$ ,  $\omega\rho$  and  $a_0(980)\sigma$ . If  $\omega\rho$  is the only strong decay channel, it restricts the maximum possible full-width severely. This is because the rapid increase in  $\rho_{\omega\rho}$  with  $s$  inflates

the Breit-Wigner denominator and cuts off the upper side of the resonance. The consequence in Ref. [6] was that the optimum fitted full-width was only 110 MeV.

This width is too small for good consistency with the  $\eta\pi^0\pi^0$  data. Some other broad threshold is needed for an acceptable fit. This is provided by the  $a_0(980)\sigma$  decay. Data for  $\bar{p}p \rightarrow \eta\pi^+\pi^-\pi^+\pi^-$  at rest [9] were found to contain some  $a_0(1450)$  signal in  $\eta\pi^+\pi^-\pi^+$ , improving log likelihood by 32 for 2 fitted parameters; this is statistically  $> 7$  standard deviations. However, there was no optimum when the mass and width of  $a_0(1450)$  were scanned. The branching fraction for the  $\eta 4\pi$  final state is a factor 14 larger than for  $\eta\pi\pi$ , with the result that the allowed branching fraction of  $a_0(1450) \rightarrow a_0(980)\sigma$  could be as much as 4.3 times that of  $\eta\pi$ . It now turns out that including the  $a_0(980)\sigma$  threshold supplies the required broad component in  $a_0(1450)$  decays and improves markedly the fit reported here. The required branching ratio to  $\eta 4\pi$  is only slightly smaller than that fitted in Ref. [9], so it appears to be a genuine signal.

Ideally the  $\eta\pi^+\pi^-\pi^+\pi^-$  data should be included in the present fits. Unfortunately those data have been lost, so this is not possible without major work reprocessing them from raw data. This is not worth the effort, since they did not constrain the mass and width of  $a_0(1450)$ . All that matters is the magnitude of the fitted signal and the upper limit on the  $a_0(980)\sigma$  branching fraction; these can be taken from the earlier publication.

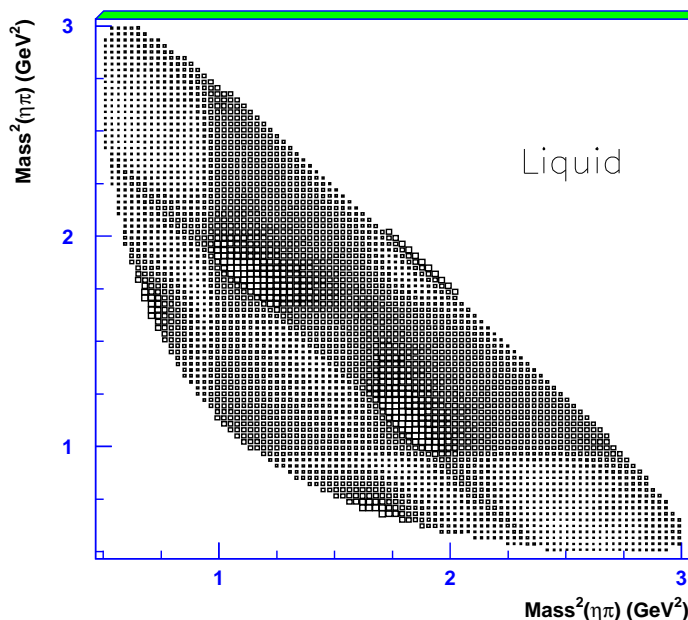


Figure 2: The Dalitz plot for  $\bar{p}p \rightarrow \eta\pi^0\pi^0$  at rest in liquid hydrogen.

### 3.1 Features of the $\eta\pi^0\pi^0$ data

The Dalitz plots for data in liquid and gaseous hydrogen are shown in binned form in Figs. 2 and 3. There are  $\sim 280,000$  events in liquid hydrogen with experimental background  $< 1\%$ . A minor detail is that any bins overlapping the edges of the Dalitz plots have been removed from Figs. 2 and 3 and the fits. There are also some further bins immediately adjoining edge bins and showing questionable behaviour. This can arise if an event lies outside the true Dalitz plot before the kinematic fit. That fit enforces the constraints of energy-momentum conservation and the masses of  $\pi^0$ ,  $\eta$  and  $\omega$ . It pulls events inside the Dalitz plot, but there is some tendency for them to congregate towards the edges. These bins are easily identified and removed because the fit is systematically lower than data. A total of 18 out of 3582 bins are removed for this reason, though effects on fitted parameters are tiny.

Statistics for  $\eta\pi\pi$  are so high ( $\sim 280,000$  events) that it was not possible to equal those statistics in the Monte Carlo simulation. (Only a few per-cent of events survive the data selection). It is assumed that the acceptance is uniform, in accord with observations for present data,  $\bar{p}p \rightarrow \eta\eta\pi^0$  and  $3\pi^0$ . The final fit has a  $\chi^2$  of 2.9 per

bin. A similar value was obtained in fitting  $\bar{p}p \rightarrow 3\pi^0$  [12]. Examination of the present fit reveals no systematic deviation across the Dalitz plot associated with fitted components. There are possible slow variations with  $\chi^2$  up to 10 which could be associated with small systematic effects in the slowly varying  $\pi\pi$  S-wave or alternatively could arise from small variations in experimental acceptance. Any departure from uniform acceptance over the width of  $a_0(1450)$  has an effect much smaller than errors. However, it has been necessary to scale statistical errors to account for the mean  $\chi^2$  per bin.

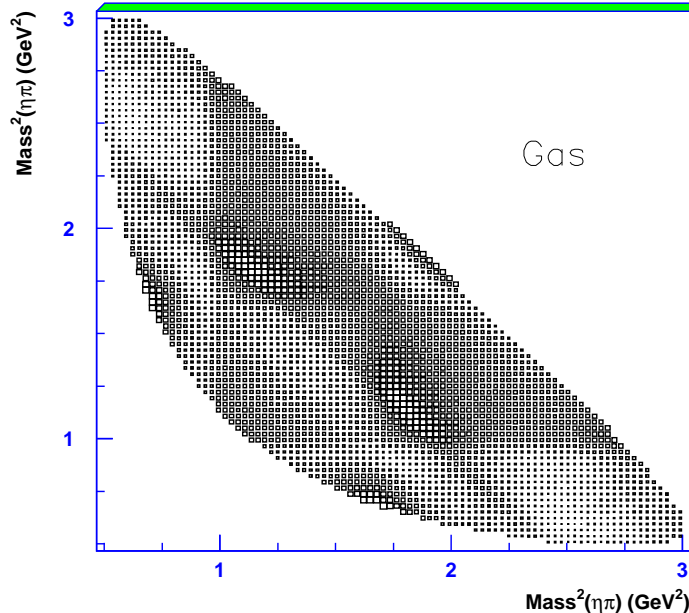


Figure 3: The Dalitz plot for  $\bar{p}p \rightarrow \eta\pi^0\pi^0$  at rest in gaseous hydrogen.

Figs. 2 and 3 resemble one another closely, showing that the effects of P-state annihilation are small. Both sets of data are fitted fully, and the final fit gives 7.4% P-state contribution, in close agreement with an earlier determination [13]. This comes mostly from  $^3P_1$  and  $^3P_2 \rightarrow a_2(1320)\pi$  and  $a_2(1700)\pi$ , and  $^3P_1 \rightarrow \eta\sigma$  and  $\eta f_0(980)$ . The former plays an important role in fitting the angular dependence of the prominent  $a_2(1320)$  bands. The effect of the latter two components is visible along the  $f_0(980)$  band, where interferences between  $f_0(980)$  and  $\sigma$  affect the apparent width of the  $f_0(980)$  in the data. Ultimately P-state annihilation has little effect on fitted parameters of either  $a_0(980)$  or  $a_0(1450)$ . P-state production of  $a_0(1450)$  is inhibited by a centrifugal barrier and makes only a very weak contribution (0.27%).

The two  $a_2(1320)$  bands interfere constructively at the upper right-hand edge of the Dalitz plots. Interference between the two  $a_2$ 's builds a bridge between them along this edge. The bands appear to be not quite vertical/horizontal. In the analyses of the 1990's, this deviation was fitted by a broad  $\eta\pi$  P-wave resonance with ill-defined mass and a large width of  $\sim 600$  MeV. Those parameters are inconsistent with what is now known about the  $\eta\pi$  P-wave. The current fits are made with the  $\pi_1(1400)$  parameters fitted to Crystal Barrel data on  $\bar{p}n \rightarrow \pi^-\pi^0\eta$  [14]. In those data, there is a significant P-state contribution because the process  $^1P_1 \rightarrow \pi\pi_1(1400)$  goes via the S-wave. In present  $\eta\pi^0\pi^0$  data, there is now a small (0.9%) P-state contribution from  $\pi(1400)$  and only 0.6% in S-state annihilation.

Another distinctive feature of the Dalitz plots is a sharp 'edge' in  $\eta\pi$  coinciding accurately with the  $KK$  threshold. This is due to the opening of the  $KK$  threshold for  $a_0(980)$ . At this threshold,  $\rho_{KK}$  changes from real to imaginary as one crosses the threshold from above to below. The amplitude for  $a_0(980)$  therefore turns in phase by  $90^\circ$ . Consequently, interference with the  $\pi\pi$  S-wave changes dramatically. The precise form of the 'edge' is therefore sensitive to the relative coupling of  $a_0(980)$  between  $\eta\pi$  and  $KK$ .

Fig. 4 shows mass projections for  $\pi^0\pi^0$  and  $\eta\pi^0$  in liquid hydrogen and the fit. Fig. 4(b) is the easier to understand. The first (left-hand) peak is a reflection of the  $a_2(1320)$  at the left-hand side of the Dalitz plot. The sharp rise to the second peak is caused by the 'edge' due to  $a_0(980)$  and its interferences with  $a_2(1320)$ . The third peak is directly due to  $a_2(1320)$ . The sudden drop at high mass is due to the  $a_2(980)$  'edge' crossing

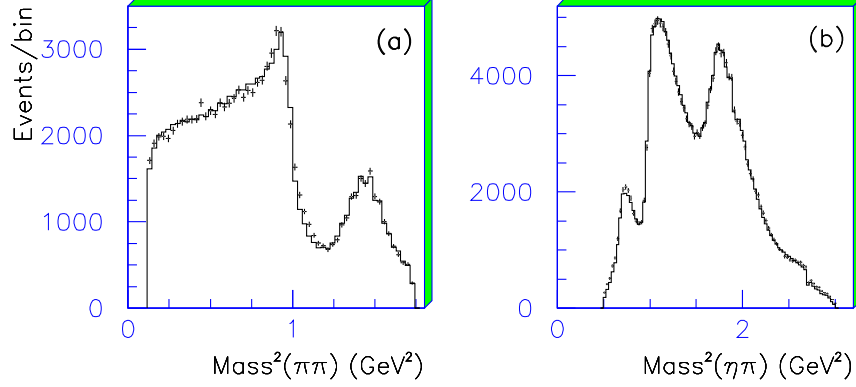


Figure 4: Mass projections for (a)  $\pi\pi$  and (b)  $\eta\pi$  for  $\bar{p}p \rightarrow \eta\pi^0\pi^0$  at rest. Points with errors show the data; histograms show the fit.

the right-hand side of the Dalitz plot. The quality of the data (and fit) illustrate the information available on  $a_0(980)$  and its coupling to  $KK$ . Note that the  $a_0(1450)$  is not directly visible in Fig. 4(b).

In Fig. 4(a), there is one high point at  $s_{\pi\pi} = 0.44 \text{ GeV}^2$ . It does not correlate with anything and appears to be a statistical storm. The first peak to its right is again due to  $a_0(980)$  and its interferences with  $a_2(1320)$  and the  $\pi\pi$  S-wave. The second peak is a reflection of  $a_2(1320)$  on the lower side of the Dalitz plot.

The cusp in  $a_0(980)$  at the  $KK$  threshold is sufficiently narrow that it is necessary to fold in the mass resolution for bins adjoining the  $KK$  threshold. The mass resolution is a Gaussian with a  $\sigma$  of 9.5 MeV. This number is derived from data on  $\bar{p}p \rightarrow \pi^0\eta'(958)$  [15], where the fitted width of the  $\eta'$  is readily measured. The folding is done using Gaussian 12 point integration over the bins concerned.

### 3.2 The $\pi\pi$ S-wave amplitude

This is the third major component in the  $\eta\pi^0\pi^0$  data. Since the earliest publications in the 1990's, our knowledge of the  $\pi\pi$  S-wave amplitude has improved greatly. Today, the  $\sigma$  pole is well known from (a) the BES2 data on  $J/\Psi \rightarrow \omega\pi^+\pi^-$ , where it produces a strong peak at  $\sim 500 \text{ MeV}$  [16], (b) the calculations of Caprini, Colangelo and Leutwyler using the Roy equations to constrain the  $s$ -dependence of the elastic amplitude [17].

The  $\pi\pi$  elastic scattering amplitude may be written in the form

$$f_{el}(s) = N(s)/D(s), \quad (7)$$

where  $N(s)$  is real and must be equal to  $-\text{Im}D(s)$  below the  $KK$  threshold. In a production reaction,  $D(s)$  must be the same for the  $\sigma$  pole as in elastic scattering (Watson's theorem [18]). However,  $N(s)$  is allowed to be quite different between production and elastic scattering [19]. The strong peak close to 500 MeV in BES data for  $J/\Psi \rightarrow \omega\pi^+\pi^-$  is fitted accurately taking  $N(s)$  to be constant. There is then accurate agreement [20] between the pole observed in these data and the elastic phase shifts predicted by Caprini et al.

The recent fits to data on  $\bar{p}p \rightarrow 3\pi^0$  [12] require a 2-component form for the S-wave production amplitude:

$$f_{prod} = \Lambda_1 f_{el}(s) + \Lambda_2/D(s), \quad (8)$$

where  $\Lambda_{1,2}$  are complex coupling constants: i.e. a coherent sum of the elastic amplitude and the pole term. This 2-component prescription also fits the  $\eta\pi^0\pi^0$  data, with different  $\Lambda$  to those for  $\bar{p}p \rightarrow 3\pi^0$ . This prescription will play an essential role throughout the present work, including the fit to data on  $\bar{p}p \rightarrow K_L^0 K^\pm \pi^\mp$  where both the  $\kappa$  pole and the elastic  $K\pi$  amplitude contribute. Similar variations of the  $\pi\pi$  S-wave amplitude are well known in decays of  $\Upsilon'$  to  $\Upsilon\pi\pi$  and are discussed in detail by Simonov and Veselov [21].

Two alternative prescriptions are available for the  $\pi\pi$  S-wave, from Refs. [20] and [12]. The latter is fitted to data for  $\bar{p}p \rightarrow 3\pi^0$ , where the  $\pi\pi$  mass range extends to 1.74 GeV. For  $\bar{p}p \rightarrow \eta\pi^0\pi^0$ , the  $\pi\pi$  mass range stops at 1.329 GeV. The  $4\pi$  inelasticity is quite small up to this mass. The two alternatives lead to only minor differences in the quality of fit to  $\bar{p}p \rightarrow \eta\pi^0\pi^0$ . The first prescription is simpler and faster and is used for final fits.

A question arises whether to assume the  $a_0(980)\sigma$  channel is produced via the  $\sigma$  pole or the elastic  $\pi\pi$  amplitude. If the latter is used,  $a_0(980)\sigma$  phase space rises too slowly to have much effect over the mass range of  $a_0(1450)$ . Some production of the  $\pi\pi$  S-wave via its pole term is needed and is what is used here. It is also what was fitted to  $\eta 4\pi$  data. The mean mass of the  $\sigma$  is then  $\sim 470$  MeV and the full width is  $\sim 500$  MeV. The  $a_0\sigma$  phase space is then substantial at 1450 MeV.

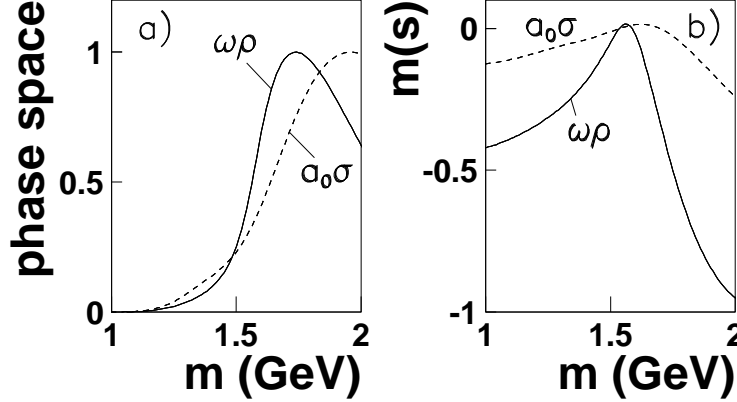


Figure 5: (a) Phase space for  $\omega\rho$  (full curve) and  $a_0(980)\sigma$  (dashed); (b) contributions to  $\text{Re } \Pi(s)$  for  $a_0(1450)$ .

Fig. 5(a) shows  $\omega\rho$  and  $a_0(980)\sigma$  phase space. They both peak in the mass range 1.65–2.0 GeV because of the form factor. Fig. 5(b) shows the subtracted form  $m(s) = \text{Re } \Pi(s) - \text{Re } \Pi(M^2)$  for  $a_0(1450)$  with the normalisation of final fits. To a first approximation, they are proportional to the gradient of phase space. Their sum is roughly half the magnitude of  $M^2 - s$ , so their effects on the line-shape of the resonance are quite large.

### 3.3 Treatment of $f_0(980)$

A further element required to fit the  $\eta\pi^0\pi^0$  data is from  $f_0(980)$ . A full re-analysis of  $f_0(980)$  parameters including the dispersive effect is a major undertaking requiring fits to the many sets of data in which it is prominent. For present data, the line-shape of  $f_0(980)$  is not critical. Fig. 6(b) below will illustrate the blurring of the threshold cusp in  $a_0(980)$  due to mass resolution. The blurring is even more severe for  $f_0(980)$ , which has a full-width at half-maximum of  $34 \pm 8$  MeV [22], compared with the mass resolution of  $\pm 9.5$  MeV. The mass resolution is folded with the line-shape of  $f_0(980)$  in the fit to data. The effect of the threshold cusp is a marginal decrease in the width compared with the BES parametrisation. This small perturbation has negligible effect on the parameters fitted to  $a_0(980)$  and  $a_0(1450)$ , because information on these two resonances comes from regions of the Dalitz plot having only modest overlap with  $f_0(980)$ .

### 3.4 Fits to $a_0(1450)$

Fits have been made simultaneously to the four set of data listed in the Abstract. The precise formula fitted to  $a_0(1450)$  needs discussion. A form factor is needed in calculating dispersive terms, in order to make the dispersion integrals converge. However, as Fig. 5(a) shows, the form factor plays a strong role only above 1650 MeV, well above the  $a_0(1450)$ . The form factor is therefore an unnecessary elaboration over the mass range covered by  $a_0(1450)$ . For simplicity, it is therefore dropped in the amplitude fitted to data.

The  $a_0(1450)$  amplitude may be written

$$f(1450) = 1/[M^2 - s - (\Pi(s) - \Pi(M^2)) - i \sum_j g_j^2 \rho_j(s)], \quad (9)$$

where the sum runs over  $\eta\pi$ ,  $KK$ ,  $\eta'\pi$ ,  $\omega\rho$  and  $a_0(980)\sigma$  channels. A slightly rearranged formula will be given later in the light of observed results. Values of  $g^2$  for  $KK$  and  $\eta'\pi$  at the peak (i.e. near the pole) will be fixed to SU(3) predictions, which depend on the angle  $\phi = 54.7^\circ - \Theta_{PS}$ , where  $\Theta_{PS}$  is the pseudoscalar mixing angle. Values of  $\phi$  may be obtained from analysis of radiative decays of vector (V) and pseudoscalar mesons

(P) mesons. Escribano and Nadal analyse all existing data and conclude there is no significant evidence for a gluonic component in  $\eta$  or  $\eta'$  [23]. It seems prudent to use results without that component. They then find  $\phi = (41.5 \pm 1.2)^\circ$ . Thomas does a similar analysis with an identical conclusion [24]. Data on  $J/\Psi \rightarrow VP$  decays also give a less precise result:  $\phi = (40.5 \pm 2.4)^\circ$  [25]. The weighted mean  $\phi = (41.3 \pm 1.2)^\circ$  will be used here. Then

$$g_{\eta'\pi}^2/g_{\eta\pi}^2 = \tan^2 \phi = 0.772 \pm 0.068, \quad (10)$$

$$g_{KK}^2/g_{\eta\pi}^2 = 1/(2 \cos^2 \phi) = 0.886 \pm 0.034. \quad (11)$$

### 3.5 Treatment of branching ratios

The relative value  $g_{\omega\rho}^2/g_{\eta\pi}^2$  is obtained from relative branching fractions of  $a_0(1450)$  in  $\eta\pi\pi$  and  $\omega\rho\pi$  data. However there are two points which need to be taken into account.

Firstly, the observed branching fractions for each resonance in  $\bar{p}p$  data must be obtained by folding the phase space factors for each channel with the line-shape of the resonance, using integrals of the form

$$I_j = \int \frac{ds g_j^2(s) \rho_j(s) k'}{|D(s)|^2}. \quad (12)$$

The factor  $k'$  is the momentum with which the resonance is produced in  $\bar{p}p \rightarrow \pi + a_0(1450)$ ; it allows for the phase space corresponding to the length of the  $a_0(1450)$  band as a function of  $s$  on the Dalitz plot.

Secondly, there is an important point of principle concerning how to account for interferences. Data are fitted including all the interferences, not only between different resonances but also including, for example, two  $a_2(1320)$  appearing in  $\eta\pi^0\pi^0$  data. The coupling constants  $\Lambda$  are determined by the fit; but then, for use in Eq. (12), intensities of individual components must be evaluated from these  $\Lambda$  without the interferences. The two  $a_2$ 's contribute 30.3% of  $\eta\pi^0\pi^0$  data, but 5.8% of this arises from interference between the two bands.

There are even larger effects for  $a_0(1450)$ . In  $\eta\pi\pi$ , there are constructive interferences between the two  $a_0(1450)$ . Including interferences, they contribute 5.44% of the cross section, but without interferences, this drops to  $A = 3.48\%$ . In  $\omega\pi^+\pi^-\pi^0$  data, there are three charge states for  $a_0$  in the amplitude ( $a_0^+\pi^- - a_0^0\pi^0 + a_0^-\pi^+$ ), where signs arise from isospin Clebsch-Gordon coefficients. There are therefore some destructive interferences. With this interference included, the  $a_0$ 's contribute 3.49% of  $\omega\rho\pi$  data, but without them  $B = 4.86\%$ . The ratio  $B/A$  determines  $3g_{\omega\rho}^2 I_{\omega\rho}/g_{\eta\pi}^2 I_{\eta\pi}$ . For the  $a_0(980)$ , interference effects are quite small, because the peak of the resonance is narrow.

It is necessary to arrange, iteratively, that the fitted branching ratio between  $\eta\pi$  and  $\omega\rho$  signals is consistent with the fitted value of  $g_{\omega\rho}^2/g_{\eta\pi}^2$ . Table 1 lists the percentages of the signals fitted to  $\eta\pi^0\pi^0$  data including interferences. These do not add up to 100% because of interferences.

signal	Percentage
$\pi\pi$ S-wave	$9.4 \pm 0.3$
$f_0(980)$	$11.7 \pm 0.2$
$a_0(980)$	$12.8 \pm 0.2$
$a_0(1450)$	$5.44 \pm 0.25$
$a_2(1320)$	$30.3 \pm 0.2$
$a_2(1700)$	$6.2 \pm 0.2$
$\pi_1(1405)$	$0.6 \pm 0.2$
P-states	$7.4 \pm 0.5$

Table 1: Intensities of signals fitted to  $\bar{p}p \rightarrow \eta\pi^0\pi^0$  data.

### 3.6 Comments on the fit to $a_0(1450)$

The fit to  $a_0(1450)$  improves significantly compared with work in the 1990's where a Breit-Wigner resonance of constant width was assumed. Parameters of  $a_0(980)$  and  $a_0(1450)$  were correlated significantly in that early work,



because the large and constant width of  $a_0(1450)$  made it overlap  $a_0(980)$  significantly. The mass of  $a_0(1450)$  could move between 1450 and 1510 MeV as  $\Gamma$  was varied. Now the width of  $a_0(1450)$  near 1 GeV is restricted to  $\eta\pi$  and  $KK$  and the width to  $\eta\pi$  is only 19 MeV at a mass of 1 GeV. The result is that  $a_0(980)$  and  $a_0(1450)$  are now almost uncorrelated. With the  $s$ -dependent forms used here, the peak position is very stable in the range 1440–1460 MeV, with an optimum at 1448 MeV.

Furthermore, the fitted  $a_0(1450) \rightarrow \eta\pi$  signal increases from 3.0% to 5.4%. The data clearly prefer the  $s$ -dependent form. The full width of  $a_0(1450)$  at half maximum decreases substantially from the  $265 \pm 13$  MeV quoted by the Particle Data Group [1] to  $192 \pm 9(\text{stat}) \pm 9(\text{syst})$  MeV. This is inevitable in view of the rapidly increasing  $a_0(980)\sigma$  and  $\omega\rho$  signals, which make the Breit-Wigner denominator cut off the line-shape at high mass. The PDG value is subject to serious systematic error from the assumption of constant width.

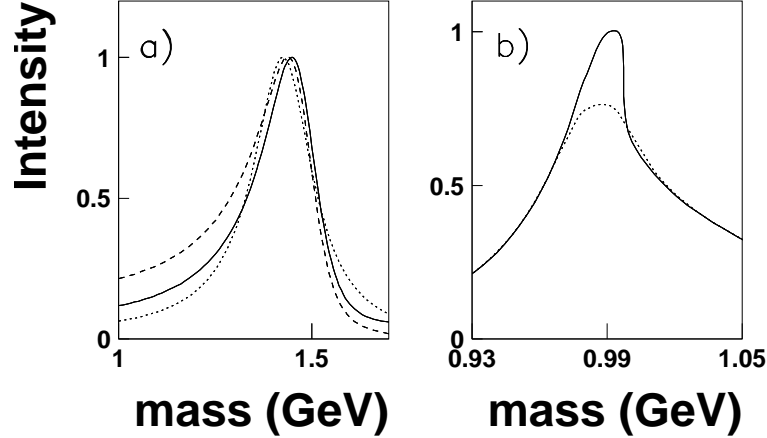


Figure 6: (a) Natural line-shape of  $a_0(1450)$  (full curve) and with the effect of  $\bar{p}p$  phase space included (dashed curve); the dotted curve shows a Breit-Wigner resonance of constant width agreeing at half-height with the full curve. (b) Natural line-shape of  $a_0(980)$  (full curve) and including the mass resolution of the Crystal Barrel detector (dotted).

The  $a_0(1450)$  line-shape for an isolated resonance, i.e. without the factor  $k'$  of Eq. (12), is shown by the full curve of Fig. 6(a). What is plotted is  $|1/D(s)|^2$ , i.e. ignoring any phase space effects in the numerator of the amplitude. The line-shape observed in  $\bar{p}p$  data including the factor  $k'$  is shown by the dashed curve. A Breit-Wigner line-shape with constant width is shown by the dotted curve, agreeing at half-height with the full curve. The true line-shape is asymmetric because of the rising phase space for  $\omega\rho$  and  $a_0(980)\sigma$  and also because of the dispersive term  $\Pi(s)$  in the Breit-Wigner denominator.

Fig. 6(b) shows the line-shape of  $a_0(980)$  without and with the effect of mass resolution of the Crystal Barrel detector. The  $a_0(980)$  is cut almost in half by the opening of the  $KK$  threshold. At this threshold, the line-shape drops rapidly because of the  $KK$  width in the Breit-Wigner denominator. Many theorists base calculations on the 50–100 MeV width of the  $a_0(980)$  quoted by the PDG. This is the full width at half-maximum. The values of  $g_{\eta\pi}^2$  and  $g_{KK}^2$  are both  $\sim 160$  MeV, comparable with other resonances.

The Argand diagram for the coherent sum of  $a_0(1450)$  and  $a_0(980)$  is shown in Fig. 7, excluding the effect of mass resolution. The maximum amplitude for  $a_0(1450)$  is at 1448 MeV, where the phase of the  $\eta\pi$  amplitude is only  $\sim 50^\circ$ . The phase goes through  $90^\circ$  only at 1536 MeV. This is the mass  $M$  in the Breit-Wigner denominator. The full curve of Fig. 8 shows the Argand diagram of  $a_0(1450)$  drawn from  $1/D(s)$  alone. It appears to lie on its side because it is cut off at high mass by the rapid increase of  $a_0\sigma$  and  $\omega\rho$  phase space. The value of  $M$  in the Breit-Wigner denominator is a derived quantity, rather strongly dependent on  $g^2(\omega\rho)$  and  $g^2(a_0(980)\sigma)$  and their form factors. Accordingly,  $M$  has a factor 2 larger error than the peak mass, which responds directly to the magnitude of the  $\eta\pi$  amplitude.

An important check is whether  $a_0(1450)$  really requires a resonant loop like that shown on Fig. 7. The first check is to replace the resonant form with its absolute magnitude, deleting its phase variation. As expected,  $\chi^2$  increases by 297.3 (after renormalising to allow for the fact that  $\chi^2$  is 2.9 per data point); this is a 17 standard deviation effect.

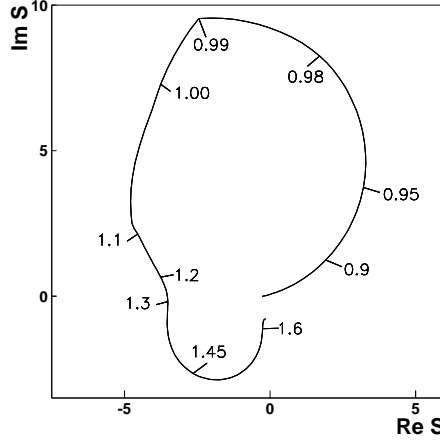


Figure 7: Argand diagram for the coherent sum of  $a_0(980)$  and  $a_0(1450)$ , excluding the effect of experimental mass resolution. Masses are shown in GeV.

A more delicate check is to break the mass range from 1315 to 1675 MeV into 30 MeV bins and optimise the  $a_0(1450)$  signal in each bin. The result is compared with the Argand diagram of  $a_0(1450)$  alone on Fig. 8. The individual bins follow the expected loop closely up to 1540 MeV; dotted lines show the movement of each bin from the analytic formula. Up to this mass, there is large interference between  $a_2(1320)$  and  $a_0(1450)$ , providing strong constraints on its phase variation with mass. Above this, three of the four remaining points show a rather large scatter. Above 1560, the effect of  $a_2(1700)$  becomes more important than that of  $a_2(1320)$ . Final fits use Crystal Barrel parameters for  $a_2(1700)$ :  $M = 1660$  MeV,  $\Gamma = 280$  MeV [26]. The main problem is that the corner of the Dalitz plot above  $m_{\eta\pi} = 1560$  MeV is a cramped area in which to separate spin zero components from spin 2. The  $a_2(1700)$  has significant contributions from all three initial states  $^1S_0$ ,  $^3P_1$  and  $^3P_2$ . These allow it to simulate a spin 0 contribution to some extent, despite the existence of the data in gas which help determine P-state contributions. The most likely explanation of the discrepancies above 1560 MeV is a poor separation between  $a_2(1700)$  and  $a_0(1450)$ .

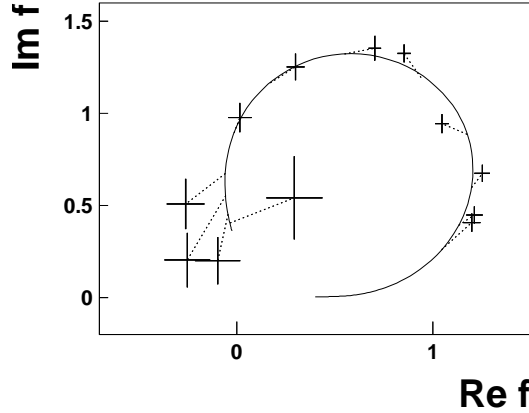


Figure 8: The Argand loop of  $a_0(1450)$  (full curve) compared with magnitude and phase for individual bins 30 MeV wide, centred at 1.33 to 1.66 GeV. Dotted lines show how individual bins move from the analytic formula.

Finding the pole position of  $a_0(1450)$  requires parametrisations of  $a_0\sigma$  and  $\rho\omega$  phase space and the dispersive term in the Breit-Wigner denominator. This has been done with three alternative parametrisations for each of the three terms. Formulae are chosen with good convergence properties for complex  $s$ , i.e. powers of  $s$  confined to the denominators of the formulae. All combinations of the formulae agree within  $\sim 3$  MeV for both real and imaginary parts of the pole, showing that systematic errors for the extrapolation are well under control. The pole position is  $1432 - i98$  MeV; the main systematic errors arise from the mean mass and width of the peak.

Fig. 9 shows as dashed curves the intensities of  $a_0(1450) \rightarrow a_0(980)\sigma$  and  $\omega\rho$  as they appear in production

from  $\bar{p}p$ . The  $a_0(980)\sigma$  decay peaks at 1458 MeV and the  $\omega\rho$  decay peaks at 1476 MeV. Curves are normalised to 1 at their peaks. Full curves show the peaks for an isolated resonance without the limitation of  $\bar{p}p$  phase space for production. The  $a_0(980)\sigma$  peak is then at 1467 MeV and the  $\omega\rho$  peak at 1485 MeV.

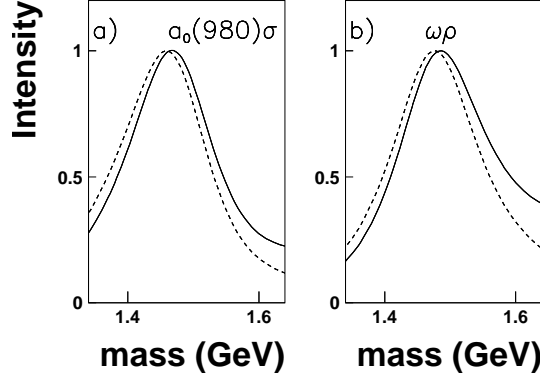


Figure 9: Line-shapes of  $a_0(1450)$  as it appears in decays to  $a_0(980)\sigma$  and  $\omega\rho$ , all normalised to 1 at the peaks. Dashed curves include the phase space for production in  $\bar{p}p$  annihilation; full curves are for an isolated resonance without the limitation of the production process.

### 3.7 Fitted parameters

Table 2 collects results for  $a_0(1450)$  from the final fit. At this point, it is necessary to present a more convenient formula for  $a_0(1450)$  than Eq. (9), and the rationale behind it.

The basic points spring from the fact that there is a pole at  $1432 - i98$  MeV. If one knew in advance how parameters vary between the pole and the physical region, it would be best to write the formula directly in terms of the pole and its residues, which express its coupling to every channel. That is not the case, so the closest approach is to write the formula in terms of the nearby peak mass,  $m_p = 1448$  MeV and widths to each channel at this mass, together with their  $s$ -dependence:

$$f(1450) = 1/[M^2 - s - i[\Pi(s) - \pi(M^2)] - im_p \sum_j \Gamma_j(s)], \quad (13)$$

$$m_p \Gamma_j(s) = g_j^2 \rho_j(s). \quad (14)$$

This form is close to that for a Breit-Wigner resonance of constant width and is closely related to observed branching ratios between channels.

The branching fractions for an isolated resonance are given by integrals of the form

$$\int \frac{g_j^2 \rho_j(s) ds}{|D(s)|^2}.$$

If  $\rho_j$ , hence  $\Gamma_j(s)$ , were to vary linearly with  $s$ , the variation of branching fractions would cancel between upper and lower halves of the peak. It turns out that this cancellation works fairly well. This form of parametrisation gives a clear insight into the way the fit responds to each parameter.

However, one important point emerges. The sum of the widths at the peak comes to 345 MeV, considerably larger than the observed full width of the peak, 192 MeV. The reasons for this are straightforward. On the lower side of the peak,  $\Gamma(a_0(980)\sigma)$  and  $\Gamma(\omega\rho)$  are small, and the amplitude falls rapidly because the remaining width to  $\eta\pi$ ,  $KK$  and  $\eta'\pi$  is small. On the upper side of the peak,  $\Gamma(a_0(980)\sigma)$  and  $\Gamma(\omega\rho)$  rapidly become large and dominate the denominator, cutting off the line-shape  $1/|D(s)|^2$  quickly. The line-shape of  $a_0(980)$  in Fig. 6(b) serves as a second example. The upper part of the peak is attenuated rapidly by  $\Gamma_{KK}(s)$ . The lower part is not far from a Breit-Wigner resonance of constant width.

The branching ratio  $\Gamma(a_0(980)\sigma)/\Gamma(\eta\pi)$  is obtained from the combined fit. It is consistent with the magnitude of the  $a_0(1450)$  signal fitted to  $\eta\pi^+\pi^-\pi^+\pi^-$  data in Ref. [9] and with the upper limit of 4.3 established there for

Peak mass	$1448 \pm 13 \pm 25$
M(Breit-Wigner)	$1536 \pm 20 \pm 30$
Mean mass	$1424 \pm 13 \pm 25$
Full width at half maximum	$192 \pm 9 \pm 9$
Pole position	$1432 \pm 13 \pm 25 - i(98 \pm 5 \pm 5)$
$\Gamma(\eta\pi)$	$23.7 \pm 0.5 \pm 2.0$
$\Gamma(KK)$ (fixed from Eq. 11)	$17.7 \pm 0.3 \pm 2.0$
$\Gamma(\eta'\pi)$ (fixed from Eq. 10)	$11.4 \pm 0.2 \pm 1.5$
$\Gamma(\omega\rho)$	$219 \pm 18 \pm 24$
$\Gamma(a_0(980)\sigma)$	$73 \pm 5 \pm 20$
In $\bar{p}p \rightarrow a_0(1450)\pi$ :	
$BR(a_0(980)\sigma)/BR(\eta\pi)$	$2.3 \pm 0.2 \pm 0.6$
$BR(\omega\rho)/BR(\eta\pi)$	$7.6 \pm 0.6 \pm 1.2$
Branching fraction in $\eta\pi^0\pi^0$ :	
(a) with interferences	$(5.44 \pm 0.15 \pm 0.88)\%$
(b) without	$(3.48 \pm 0.13 \pm 0.58)\%$
Branching fraction in $\omega\pi^+\pi^-\pi^+\pi^-$ :	
(a) with interferences	$(3.49 \pm 0.14 \pm 0.30)\%$
(b) without	$(4.86 \pm 0.19 \pm 0.42)\%$

Table 2: Results for  $a_0(1450)$  in units of MeV. The first errors are statistical and the second systematic.

this ratio. The Table uses branching ratios to  $\omega\rho$  from the combined fit to  $\omega\pi^+\pi^-\pi^0$  data, discussed in detail in subsection 3.9. The Table quotes in lines 12 and 13 the ratio of branching fractions  $BR(\omega\rho)/BR(\eta\pi)$  and  $BR(a_0(980)\sigma)/BR(\eta\pi)$  as they appear in  $\bar{p}p$  annihilation. These values are better defined than those for an isolated resonance because of uncertainty about its high mass tail, see Fig. 9. Note that  $BR(\omega\rho)/BR(\eta\pi)$  is 7.6 in Table 2, rather smaller than the ratio  $\Gamma(\omega\rho)/\Gamma(\eta\pi) = 9.2$  at the peak of  $a_0(1450)$ . This is because the  $\omega\rho$  signal in  $\bar{p}p \rightarrow a_0(1450)\pi$  is inhibited at high mass by the available phase space, as illustrated in Fig. 9(b) by the dashed curve. For an isolated resonance, the  $\omega\rho$  branching fraction is close to 9.2, but with an unknown error depending on form factors.

In Table 2, the first errors are statistical and the second systematic. Strong contributions to systematic errors arise from uncertainties in branching fractions for  $\bar{p}p \rightarrow \eta\pi^0\pi^0$  ( $\pm 5.0\%$ ) and  $\omega\pi^+\pi^-\pi^0$  ( $\pm 7.9\%$ ). However, the largest error arises from the fact that interferences within one set of data lead to a branching fraction  $\propto |\sum_i \Lambda_i f_i|^2$ , rather than  $\sum_i |\Lambda_i f_i|^2$ . Here, the sum is over resonances,  $\Lambda_i$  are coupling constants and  $f_i$  are amplitudes for each resonance. The second of these quantities is derived from  $\Lambda$  parameters fitted to the first, as explained above in subsection 3.5.

There is a potentially large error from the interference between the two components making up the  $\pi\pi$  S-wave: the  $\sigma$  pole term and the elastic component. Fortunately, the  $\eta\pi^0\pi^0$  data determine both relative magnitudes and phases of these two contributions quite well. However, it is necessary to add a systematic error to cover the change to the fit if a further term is added to the parametrisation of the  $\pi\pi$  S-wave. Here, it is chosen to be the elastic amplitude multiplied by  $s$ . There is a further small contribution to systematic errors from perturbations when small components are dropped from the fits, e.g. the weak  $\pi_1(1400)$  contributions in both  $^1S_0$  and  $^3P_1$  annihilation. Finally, in view of the scatter of the last 4 points of Fig. 8 above 1540 MeV, a systematic error is included from changes in the fit if  $a_0(1450)$  is fitted to  $\eta\pi^0\pi^0$  data only up to 1540 MeV.

Table 2 includes systematic errors in fitting  $\omega\pi^+\pi^-\pi^0$  data. The evaluation of systematic errors for these data follows the same procedure as for  $\eta\pi^0\pi^0$ . The final systematic errors are added in quadrature. It is not correct to add them linearly, as is sometimes done. The derivation of the Gaussian error distribution depends on the convolution of many box-shaped distributions.

### 3.8 A disagreement with Obelix

The Obelix group has published two claims to observe an  $a_0$  decaying to  $\eta\pi$  in the mass range 1290-1313 MeV [27] [28]. Such a resonance should be very conspicuous in Crystal Barrel data through distinctive interference with  $a_2(1320)$ . The fits reported here have been repeated (i) using an  $a_0$  in this mass range without  $a_0(1450)$  and (ii) together with  $a_0(1450)$ . When  $a_0(1450)$  is removed from the fit,  $\chi^2$  (scaled to allow for the mean  $\chi^2$  of 2.9 per bin) is worse by 528 for a reduction of six fitting parameters. This is an 18 standard deviation signal. If its mass and width are moved down to the mass range 1200-1340 MeV with a width  $\leq 120$  MeV, there is no optimum. Instead the fit moves in a few iterations towards parameters of  $a_0(1450)$ , whatever line-shape is used for  $a_0(1450)$ . If an extra  $a_0$  is added in the mass range 1280-1340 MeV, there is only a small improvement in  $\chi^2$  and again no optimum for parameters in the range claimed by Obelix. The narrow width they claim  $\sim 80$  MeV is similar to that of  $a_2(1320)$ . It appears likely that their signal was confused with P-state annihilation to  $a_2(1320)$ . The P-state annihilation is precisely identified in present work from data in hydrogen gas.

### 3.9 The fit to $\omega\pi^+\pi^-\pi^0$ data

There are 35,280 reconstructed events for these data with 8.4% experimental background, arising in the selection of the narrow  $\omega$ . The earlier analysis of these data is reported in detail in Ref. [6]. Dispersive effects were included fully and the new fit changes rather little. Table 3 lists the components in the fit and their significance levels, measured by changes in log likelihood when each component is removed from the fit and all others are re-optimised. Values of  $\chi^2$  are twice those for log likelihood for the large statistics available here.

Initial states	Channel	Intensity (%)	$\Delta\text{Ln L}$
$^1S_0$	$a_0(1450)\pi$ ,	3.5	90
	$b_1(1235)\rho$ , $b_1 \rightarrow \omega\pi$	13.2	361
	$\pi_1(1600)\pi$ , $\pi_1 \rightarrow [b_1\pi]_{L=0}$	6.6	71
	$a_2(1320)\pi$	2.0	18
	$a_2(1660)\pi$	2.4	36
$^3S_1$	All $\pi_0\pi$	16.9	505
	$a_1(1260)\pi$	0.8	48
	$a_1(1260)\omega$ , $a_1 \rightarrow \rho\pi$	23.9	377
	$a_1(1640)\pi$	5.1	271
	$a_1(1640)\pi$ , $a_1 \rightarrow b_1\pi$	1.7	45
	$\pi_1(1600)\pi$ , $\pi_1 \rightarrow [b_1\pi]_{L=0}$	2.5	50
	$\omega(1420)\pi$ , $\omega(1420) \rightarrow \omega\sigma$	1.2	8
	$\omega(1420)\pi$ , $\omega(1420) \rightarrow b_1\pi$	3.3	5
	$b_1(1235)\sigma$ , $b_1 \rightarrow \omega\pi$	1.6	57
	$\rho(1450)\sigma$ , $\rho \rightarrow b_1\pi$	0.6	94
$^3P_0$	$\pi_0\pi$	9.5	83
$^3P_1$ , $^3P_2$	$a_2(1320)$	2.5	38
	$a_2(1660)$	5.7	45

Table 3: Percentage contributions of each channel after the background subtraction. Decays are to  $\omega\rho$  unless stated otherwise. The final column shows changes in log likelihood when each channel is removed from the fit and remaining contributions are re-optimised.

In the earlier work, there was a very marginal signal due to  $a_1(1260) \rightarrow \omega\rho$ , which improved log likelihood by 24. In the latest work, it improves log likelihood by only 6 and is omitted from the fit. Likewise the earlier work included a rather marginal signal for  $\pi(1600) \rightarrow (b_1(1235)\pi)_{L=2}$ . This contribution is now small and is set to zero.

A further detail is that there are data for  $\bar{p}p \rightarrow \omega\pi^0\pi^0\pi^0$  [29]. The branching ratio for this channel is very small. These data constrain the magnitudes of the last four entries to Table 3 for  $^3S_1$ . Their phases are fitted freely. Two of them have only very small effects in the present fit.

Let us review the essential points of the analysis. There are three charge combinations of  $\pi\pi$ . As a result, individual resonances do not appear clearly in mass projections. It is necessary to rely on the amplitude analysis to locate magnitudes and phases from what it finds in 4-body phase space. That may appear questionable, but in practice works well. The fits to mass projections were shown in Fig. 2 of the earlier paper. The tiny changes in the new fit are hardly visible by eye and therefore the figures will not be repeated here.

Secondly, angular distributions depend distinctively on spins. Consider  $a_0(1450)$  as an example. The spin of the  $\omega$  lies along the normal to its decay plane. The spin of the  $\rho$  is given by the vector  $(k_1 - k_2)$ , where  $k_{1,2}$  are momenta of the pions from its decay. After Lorentz transformations to the  $\omega\rho$  rest frame, the matrix element is given by the scalar product of these two vectors. This is highly distinctive. An elementary check on formulae is that all amplitudes are orthogonal. One can test how well quantum numbers are recognised by putting deliberate errors into formulae. Generally the result is that the amplitudes drop to small values.

A third point is that the programme prints a matrix giving intensities of all components together with real and imaginary parts of all interferences. This identifies the important interferences. It is then easy to test the reliability of these interferences by plotting log likelihood against relative phases.

The magnitude of the  $a_0(1450)$  signal has decreased slightly from the earlier publication, but its significance level has improved. In the earlier work, log likelihood changed by 56 when  $a_0(1450)$  was omitted from the fit. Now it changes by 90. It is produced from the  $^1S_0$  initial state where it interferes with a large and well identified  $b_1(1235)\rho$  signal.

There is a large signal in  $^3S_1$  annihilation from  $J^{PC} = 0^{-+}$ . It peaks at 1480 MeV, quite close to  $a_0(1450)$ . One might worry that there will be cross-talk with  $a_0(1450)$ , despite the fact that the  $a_0(1450)$  is produced from the  $^1S_0$  initial state while  $0^{-+}$  is produced from  $^3S_1$ . There is no such problem. The  $0^{-+}$  component may be removed completely from the fit without any significant effect on the fitted  $a_0(1450)$  signal. In fact, the  $a_0(1450)$  is insensitive to changes in all  $^3S_1$ , and P-state amplitudes.

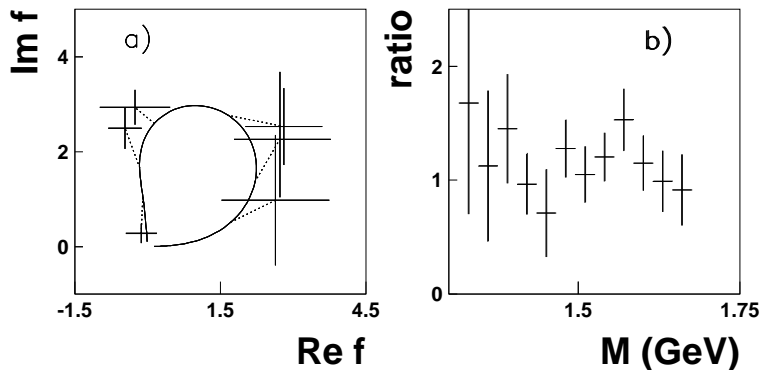


Figure 10: (a) The Argand loop of  $a_0(1450)$  in  $\omega\rho\pi$  (full curve) compared with magnitude and phase for individual bins 60 MeV wide, centred at 1.345 to 1.645 GeV. Dotted lines show how individual bins move from the analytic formula. (b) The ratio of the  $a_0(1450)$  amplitude in bins 30 MeV wide to that of the overall fit.

A similar comparison has been made in Fig. 10(a) to that shown in Fig. 8. Real and imaginary parts of the  $a_0(1450) \rightarrow \omega\rho$  signal are fitted freely in bins 60 MeV wide from 1.345 to 1.645 GeV. In Fig. 10(a), the amplitude is  $k'\sqrt{\rho_{\omega\rho}}/D(s)$ ; i.e. it allows for the phase space of the  $\omega\rho$  final state and the phase space in the production reaction  $\bar{p}p \rightarrow a_0(1450)\pi$ , proportional to the momentum  $k'$  of the  $a_0(1450)$  in the  $\bar{p}p$  centre of mass. There is no doubt that the data conform with a resonant circle, though errors are sizable. There appears to be some tendency for the data to require a larger amplitude than the overall fit. An alternative test is made by fixing the phase of the amplitude to that of the overall fit, but allowing the magnitude of the fitted signal to fit freely in 30 MeV wide bins. Fixing the phase stabilises the fitted amplitude considerably. Results are shown in Fig. 10(b). There is now a reduced tendency for the fitted amplitude to be above the overall fit. The mean discrepancy is  $(13.7 \pm 8.5)\%$ . The systematic difference arises because the final fit is constrained to fit the line-width of the  $a_0(1450)$ . If the  $a_0(1450) \rightarrow \omega\rho$  signal is increased, it makes the line-width smaller; this was the problem with the first publication, Ref. [6]. The final fit is a compromise between fitting the line-shape and the magnitude of the  $a_0(1450) \rightarrow \omega\rho$  signal.

In assessing the errors for  $\Gamma(\omega\rho)/\Gamma(\eta\pi)$  in Table 2, the statistical error is taken from the 8.5% statistical error in the discrepancy of Fig. 10(b). This is quite close to the error derived from log likelihood in Table 3. The systematic error is derived from changes in  $\Gamma(\omega\rho)/\Gamma(\eta\pi)$  as the mass and width of  $a_0(1450)$  are varied over the range of systematic errors in Table 2.

One new point does emerge from a better understanding of dispersive effects. This concerns the large  $J^P = 0^{-+}$  component. In the earlier work, attempts were made to fit it with  $\pi(1300)$  and a radial recurrence in the mass range 1600-1700 MeV. However, the required signal for  $\pi(1300)$  was unreasonably large and would have required it to decay dominantly to  $\omega\rho$ . Furthermore, the data still required a definite peak in the vicinity of 1500 MeV. A radial recurrence so close to  $\pi(1300)$  would be surprising.

The present work reveals a more sensible way of fitting the  $0^-$  signal. The optimum fit is obtained with a broad resonance at 1540 MeV with  $\Gamma = 590$  MeV, plus a radial excitation of  $\pi(1300)$  at  $1732 \pm 32$  MeV with  $\Gamma = 252 \pm 30$  MeV. The broad resonance is close to being a simple cusp at the  $\omega\rho$  threshold. This solution is shown in Fig. 11.

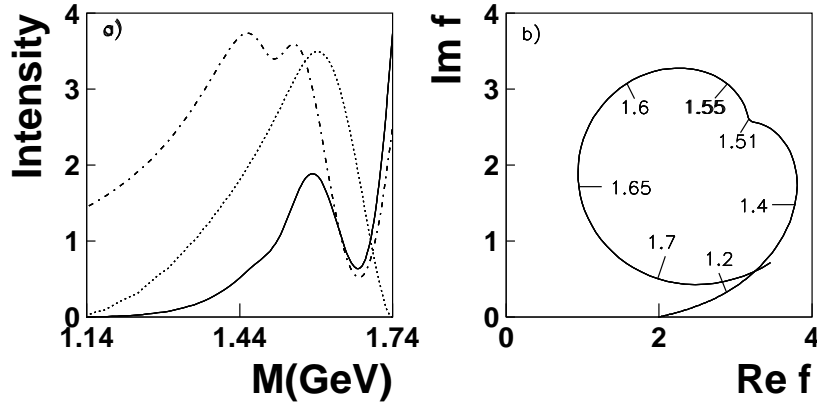


Figure 11: (a) The line-shape of the  $J^{PC} = 0^{-+}$  signal as it would appear in  $\omega\rho$  without the limitation of production in  $\bar{p}p \rightarrow \omega\rho\pi$  but (i) including  $\omega\rho$  phase space (full curve) and (ii) with this phase space factored out (chain curve). The dotted curve shows the phase space for  $\omega\rho$  including the limitation due to production in  $\bar{p}p \rightarrow \omega\rho\pi$ . (b) The Argand diagram; masses are shown in GeV. Units are arbitrary for display purposes.

Fig. 11(a) shows as the full curve the intensity of the fitted  $\omega\rho$  signal including  $\omega\rho$  phase space, for a resonance ‘in free space’, i.e. without the limitation imposed by production in  $\bar{p}p \rightarrow \omega\rho\pi$ . The phase space for  $\bar{p}p \rightarrow \omega\rho\pi$  including this limitation is shown by the dotted curve. What is actually observed in  $\omega\pi^+\pi^-\pi^0$  data is then given by the product of the dotted curve and the full curve. The chain curve shows the result of dividing the full curve by  $\omega\rho$  phase space. This result shows the line-shape arising from  $|\Lambda_A/D_A(s) + \Lambda_B/D_B(s)|^2$ , where  $A$  and  $B$  refer to the two components and  $\Lambda$  are coupling constants. This is what one would see for an isolated resonance if there were no phase space factor in the numerator. The double peak near 1.45 GeV comes from the cusp + interference. The peak at high mass comes from the radial recurrence at 1732 MeV.

Minor variants on this solution are possible because the  $\omega\rho$  amplitude below 1450 MeV is small and poorly determined, particularly its phase. One should therefore not place any reliance on the threshold behaviour of the  $\omega\rho$  amplitude below 1450 MeV. It is quite possible that the double peak at 1430 and 1480 is an artefact. However, there are two essential features which are unavoidable. The first is a peak at  $\sim 1550$  MeV in  $\omega\rho$ . This arises from the cusp at the  $\omega\rho$  threshold. The second well determined feature is the phase advance  $> 180^\circ$  from 1510 to 1740 MeV. This arises largely from the radial recurrence at 1732 MeV.

The present data are limited by the fact that production of  $0^-$  from  $^3S_1$  is suppressed at the highest masses by the  $L = 1$  centrifugal barrier for production. A quite significant signal is however observed also in P-state production with  $L = 0$ . This signal gives a reasonable determination of the mass and width of the upper resonance at 1732 MeV.

There is some chance that this radial excitation corresponds to  $\pi(1800)$ . However, using PDG parameters for  $\pi(1800)$ , the fit is 2.8 standard deviations worse than with a free fit. The mass and width observed in the present fit correspond closely to those observed by Amelin et al. in  $\pi^- A \rightarrow \omega\pi^-\pi^0 A^*$  [31]. The ideogram shown by the PDG for the mass of  $\pi(1800)$  has a double-humped structure. There is the possibility of a  $0^-$  hybrid in

this mass range to accompany the  $\pi_1(1600)$ . So there is room for a conventional radial excitation around 1730 MeV and a hybrid at higher mass. The  $\pi(1800)$  has decay modes suggestive of a hybrid. A fit using a mass and width from the higher lobe of the PDG's ideogram is worse than the free fit by 4.0 standard deviations. Further exploration of  $0^-$  signals is needed in this mass range to resolve the current uncertainties.

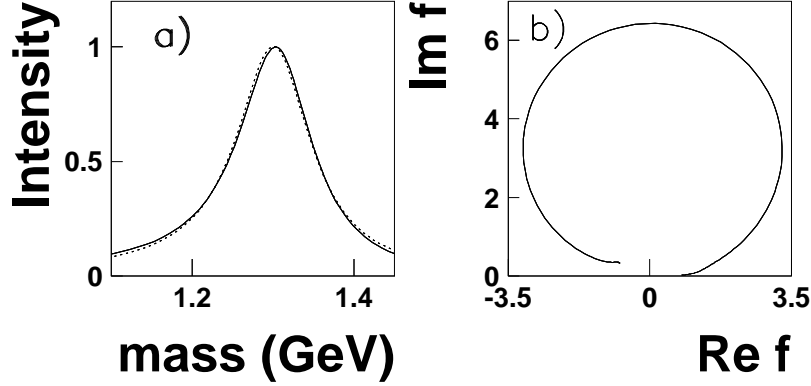


Figure 12: (a) The line-shape of  $a_2(1320)$ : full curve including  $s$ -dependence of the width and dispersive effects in full, the dotted curve showing a Breit-Wigner amplitude of constant width. (b) The Argand diagram.

A final detail concerns  $a_2(1320)$ . Fig. 12 illustrates the small effect on  $a_2(1320)$  of the  $s$ -dependence of the width and dispersive effects. The full  $s$ -dependence of decays to  $\rho\pi$ ,  $\eta\pi$ ,  $KK$  and  $\omega\rho$  is included. The full curve on Fig. 12(a) shows the fitted line-width and the dotted curve the line-shape of a Breit-Wigner amplitude of constant width agreeing at half-height with the full curve. There is little difference between them, showing that the slow  $s$ -dependence of the dominant  $\rho\pi$  channel has little effect. Fig. 12(b) shows that the Argand diagram follows a circle closely.

## 4 Results for $a_0(980)$

In the 1994 work [3], the  $a_0(980)$  was fitted with a Flatté formula with  $M = 999 \pm 5$  MeV,  $g^2(\eta\pi) = 221 \pm 20$  MeV and  $g^2(KK)/g^2(\eta\pi) = 1.16 \pm 0.18$ . The  $\eta'\pi$  channel was not included. These parameters now change beyond their errors because (a) the large dispersive cusp at the  $KK$  threshold is included, (b) Adler zeros are included in both  $\eta\pi$  and  $\eta'\pi$  channels. These are at  $s = s_A = m_\eta^2 - 0.5m_\pi^2 = 0.2905$  GeV<sup>2</sup> for the  $\eta\pi$  channel and at  $s = s_{A'} = m_{\eta'}^2 - 0.5m_\pi^2 = 0.9078$  GeV<sup>2</sup> for the  $\eta'\pi$  channel. Note that the latter is quite close to the resonance mass.

The formulae used for coupling to  $\eta\pi$  and  $\eta'\pi$  are

$$g_{\eta\pi}^2(s) = g_{\eta\pi}^2(4m_K^2) \frac{s - s_A}{4m_K^2 - s_A} \exp(-2\alpha k_\eta^2), \quad (15)$$

$$g_{\eta'\pi}^2(s) = g_{\eta'\pi}^2(m_{\eta'} + m_\pi)^2 \frac{s - s_{A'}}{(m_{\eta'} + m_\pi)^2 - s_{A'}} \exp(-2\alpha k_{\eta'}^2), \quad (16)$$

where  $k_{\eta'}$  is the momentum in the  $\eta'\pi$  rest frame. The value of  $g_{\eta'\pi}^2$  is normalised at the  $\eta'\pi$  threshold.

Below the thresholds for these processes, the Flatté formula has the sub-threshold analytic continuation

$$g_{\eta'\pi}^2 \rho_{\eta'\pi} \rightarrow ig_{\eta'\pi}^2 2|k_{\eta'}^2|/s. \quad (17)$$

However,  $g_{\eta'\pi}^2$  becomes real again for a mass  $< 0.83$  GeV, due to the opening of the  $u$ -channel. It makes little sense to allow for this without including the dynamics of the  $u$ -channel process. Therefore  $g_{\eta'\pi}^2$  is set to zero below  $s = s_{A'}$ . The effect of the  $\eta'$  channel on  $\chi^2$  of the fit is quite small, except above the  $\eta'\pi$  threshold. Its coupling constant is fixed to that of the  $\eta\pi$  channel by Eq. (10). Note that the assumption is made in Eq. (16) that the form factor does not affect the ratio  $g_{\eta'\pi}^2/g_{\eta\pi}^2$  between these two thresholds. Because of the small effect



of the  $\eta'\pi$  channel on present fits, this assumption has little effect on  $\chi^2$ . However, it could matter if and when data become available directly on the  $\eta'\pi$  channel. A detail is that the opening of the  $\eta'\pi$  channel is visible on the Argand diagram of Fig. 7, just below 1.1 GeV.

For the  $KK$  channel, the Adler zero is far away at  $s = 0.5m_K^2$  and experience with the  $\sigma$  amplitude is that the factor  $(s - s_A)/(4m_K^2 - s)$  needs to be multiplied by an exponential form factor  $\exp(-\alpha s)$ , which prevents the amplitude rising indefinitely with  $s$ . Below the  $KK$  threshold, the  $KK$  channel has only an indirect effect on data in the  $\eta\pi$  channel. Tests have been made with a variety of form factors. Within errors, the best fit is obtained with  $g_{KK}^2 = \text{constant}$  below the  $KK$  threshold and this simple prescription has been adopted. Above the  $KK$  threshold, the factor due to the Adler zero is dropped and the form factor  $\exp(-2k_{KK}^2)$  is used, with  $k_{KK}$  the momentum in the  $KK$  channel in GeV/c.

#### 4.1 Fits to $\eta\pi^0\pi^0$ data

The dispersive cusp locks the mass  $M$  of the amplitude at or just below the  $KK$  threshold and provides considerable stability. Values of  $g_{\eta\pi}^2$  and the ratio  $r_{KK} = g_{KK}^2/g_{\eta\pi}^2$  are only slightly correlated in fitting  $\eta\pi\pi$  data; there is a weak tendency (5%) for them to go up and down together. The data give well defined values for parameters of  $a_0(980)$ :

$$M = 0.9874 \pm 0.0010(\text{stat}) \pm 0.0030(\text{syst}) \text{ GeV}, \quad (18)$$

$$g_{\eta\pi}^2 = 0.164 \pm 0.007 \pm 0.010 \text{ GeV}^2, \quad (19)$$

$$r_{KK} = \frac{g_{KK}^2}{g_{\eta\pi}^2} = 1.05 \pm 0.07 \pm 0.05. \quad (20)$$

These values have changed from earlier publications because of the inclusion of the cusp in  $\text{Re}\Pi(s)$ . The ‘edge’ observed in the  $\eta\pi\pi$  data due to  $a_0(980)$  provides a good determination of the coupling to  $KK$ . In this respect, Crystal Barrel data have an advantage over Kloe data (to be discussed further below). The Kloe data however provide an excellent view of the  $a_0(980)$  line-shape below the  $KK$  threshold. A simple program evaluating the formulae for  $a_0(980)$  and the cusp in  $\text{Re}\Pi(s)$  is available from the author.

The systematic error on the mass  $M$  arises from uncertainty in the mass calibration of the Crystal Barrel detector. Systematic errors for  $g_{\eta\pi}^2$  and  $r_{KK}$  arise as described above for the entire fit to  $\eta\pi^0\pi^0$  data. The fitted mass of  $a_0(980)$  is close to the lowest  $KK$  threshold, just as the mass of  $X(3872)$  is close to the threshold of the lowest charge combination in  $\bar{D}D^*$ .

An important detail is that the  $a_0(980)$  could be produced either by its pole term or via the elastic  $\eta\pi$  amplitude. Both have been tried, and the fit strongly prefers production via the elastic scattering amplitude, i.e. with the Adler zero in the numerator of the production amplitude.

## 5 Data for $\bar{p}p \rightarrow K_L^0 K^\pm \pi^\mp$

The Dalitz plot for these data in liquid hydrogen is shown in Fig. 13. There are prominent vertical and horizontal bands due to  $K^*(890)$ . A detail is that it is necessary to fine-tune the masses and widths of the separate charge states for  $K^*(890)$ . There are also diagonal bands due to  $a_2(1320)$  and  $a_0(980)$ . The  $a_0(1450)$  lies in the lower left corner of the plot, near the crossing  $K^*(890)$  bands. As for  $\bar{p}p \rightarrow \eta\pi^0\pi^0$ , it is necessary to remove some edge bins. There is also a background from  $\bar{p}p \rightarrow \pi^+\pi^-\pi^0$  described in the Crystal Barrel publication. It peaks in edge bins close to the left-hand corner of the Dalitz plot. It is necessary to remove 21 bins, leaving 741.

One would hope to determine the ratio  $g_{KK}^2/g_{\eta\pi}^2$  for  $a_0(980)$  from relative contributions in  $\eta\pi\pi$  and  $K\bar{K}\pi$  data. Unfortunately, when one tries to do this, a serious difficulty appears. It arises from the question of how to parametrise the  $K\pi$  S-wave amplitude in the  $K\bar{K}\pi$  data. This leads to uncertainties in interferences between the  $K\pi$  S-wave and diagonal bands due to  $a_2(1320)$ ,  $a_0(980)$  and  $a_0(1450)$ . Uncertainties in these interferences then lead to uncertainties in the magnitudes of the  $a_2$  and  $a_0$  signals. To grasp these points, it is necessary to review current understanding of the  $K\pi$  S-wave, which has advanced a long way since the earlier analysis of the Crystal Barrel data [7].

In that early analysis, it was assumed that the  $K\pi$  S-wave amplitude in production data is identical to that in  $K\pi$  elastic scattering. Experience with  $\pi\pi$  data now makes that appear unlikely [19]. The Crystal Barrel paper

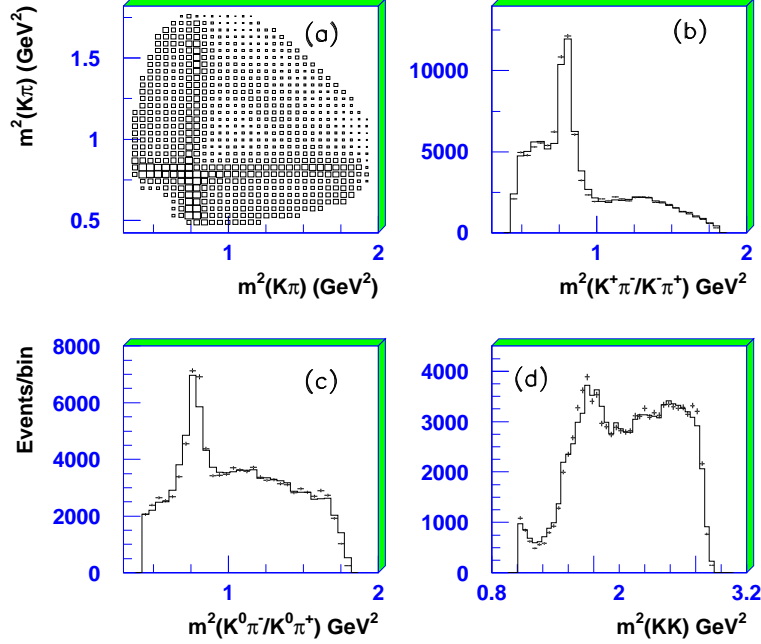


Figure 13: Data and fits for  $\bar{p}p \rightarrow K_L^0 K^\pm \pi^\mp$  at rest. (a) Dalitz plot; mass projections for (b)  $K^+\pi^-$  and  $K^-\pi^+$ , (c)  $K_L^0\pi^-$  and  $K_L^0\pi^+$ , (d)  $K_L^0 K^\pm$ . Points with errors show data and histograms show the fit.

gives an explicit parametrisation for the  $K\pi$  S-wave. Fig. 14 shows its phase as a function of mass, compared to LASS data [32]. In those days, the LASS data were fitted with an effective range expression. Since then, it has been recognised that Chiral Symmetry breaking produces an Adler zero in the  $K\pi$  S-wave below threshold at  $s = m_K^2 - 0.5m_\pi^2$ . The dashed curve shows the amplitude fitted to the LASS data including this Adler zero [33]. The  $\kappa$  pole observed in BES2 [34] and E791 [35] data was fitted simultaneously and is therefore well constrained. There is a discrepancy for  $K\pi$  masses near 1400 MeV. It is now known that this discrepancy can be removed by a full treatment of the cusp at the  $K\eta'$  threshold. For present purposes it is irrelevant since  $KK\pi$  phase space ends at 1381 MeV.

The discrepancy near the  $K\pi$  threshold between the dashed and full curves on Fig. 14 indicates a contribution in Crystal Barrel data from the  $\kappa$  pole, which peaks near threshold with a half-width of  $\sim 350$  MeV. This is confirmed by a fit to the Crystal Barrel data using a 2-component fit to the  $K\pi$  S-wave, as in Eq. (8). It contains one component from  $K\pi$  elastic scattering and a second from the  $\kappa$  pole. Uncertainties are compounded by the fact that there are contributions from  $\kappa\pi$  for both  $I = 1$  and  $I = 0$  initial states, making four  $K\pi$  S-wave amplitudes in all. These two isospins have opposite relative signs for coupling to  $K\pi$  and are responsible for the difference in  $K\pi$  distributions between Figs. 13(a) and (b).

There is in addition the possibility of a third component due to a  $K_0(1430)$  amplitude different in magnitude and phase in production data and LASS data. That is the case for the E791 data. However, it turns out that adding this freedom only improves  $\chi^2$  by a small amount,  $\sim 20$  and leads to a very ill-defined fit. This extra possible freedom is ignored here.

The earlier Crystal Barrel analysis recognised the need for a low mass  $K\pi$  enhancement and parametrised it in an *ad hoc* way which is not consistent with Chiral Symmetry breaking and the Adler zero. In order to get an acceptable fit, contributions were introduced from  $\rho(1450)$  and/or  $\rho(1700)$ , which can appear in the left-hand corner of the Dalitz plot, in the same mass range as the  $\kappa$  pole and  $a_0(1450)$ . It is now necessary to try to disentangle the complications of this corner of the Dalitz plot. Unfortunately, these complications lead to substantial errors in branching ratios.

Results will be presented first without any contribution from  $\rho(1450)$  and  $\rho(1700)$ ; then their possible contributions will be discussed. Either way, there is a large interference between the  $\kappa$  pole and the  $K\pi$  elastic

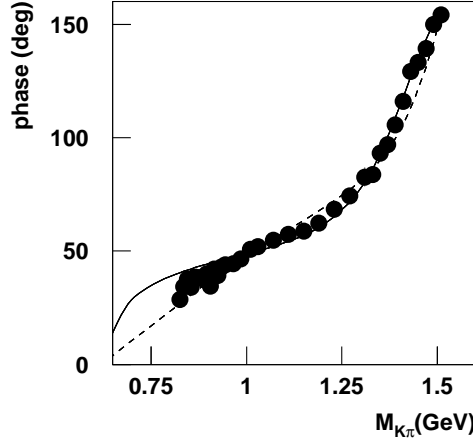


Figure 14: LASS data for  $K\pi$  elastic scattering, compared with (i) the Crystal Barrel fit (full curve), (ii) a parametrisation including the Adler zero in  $K\pi$  (dashed curve).

amplitude. With this freedom, there is great flexibility in what can be fitted to the  $K\pi$  S-wave. A free fit to  $a_0(980)$  and  $a_2(1320)$  magnitudes gives  $\chi^2 = 637.3$  for 720 degrees of freedom. If the  $\kappa$  pole is omitted,  $\chi^2 \rightarrow 1230$ ; this is clearly unacceptable. The free fit gives a ratio of intensities  $a_0(980)/a_2(1320) = 0.0637$  compared with a prediction from fits to  $\eta\pi\pi$  data, Eqs. (18-20), giving a ratio  $0.0369 \pm 0.0068$ . This might appear to be a large discrepancy. However, if the fit is constrained to agree with the latter prediction,  $\chi^2$  increases by only 2.01 to 639.31, for 2 parameters determining the complex coupling constant  $\Lambda$  of  $a_0(980)$ . There is clearly no disagreement with the prediction; there is just a large flexibility in the amplitudes.

The same picture emerges for the ratio of intensities for  $a_0(1450)/a_2(1320)$ . A free fit to  $a_0(1450)$  gives a ratio of intensities  $a_0(980)/a_2(1320) = 0.535$  compared with its predicted value 0.311. However, again the ratio can be fixed to the prediction with a  $\chi^2$  increase of only 2.01 for 2 less parameters for  $\Lambda_{1450}$ .

With the introduction of extra contributions from  $\rho(1450)$  and/or  $\rho(1700)$  the situation is similar. If both are introduced, the solution becomes very unstable with excessively large contributions from both resonances and destructive interference between them. This destructive interference is a familiar symptom of over-fitting the data, so it is necessary to use only one of them. That procedure was adopted in the earlier Crystal Barrel analysis. There are recent data from Babar [36] on  $e^+e^- \rightarrow \gamma K^+ K^- \pi^0$  using Initial State Radiation. They observe the same instability between  $\rho(1450)$  and  $\rho(1700)$  contributions, but a dominant  $\rho(1450)$  amplitude. Following this lead, the present data are fitted including only  $\rho(1450)$ . The story which then emerges runs close to that described above. For a fit where  $a_0(1450)$  and  $a_0(980)$  are constrained to predictions from Eqs. (18-20),  $\chi^2$  drops from 639.31 to 616.50 with the addition of  $a_0(1450)$ . If  $a_0(980)$  is set free,  $\chi^2$  improves by 3.09 to 613.41. This cannot be regarded as a significant improvement. If  $a_0(1450)$  is set free, the improvement is only 1.74, again insignificant.

So the conclusion is that data on  $\bar{p}p \rightarrow K_L^0 K^\pm \pi^\mp$  are consistent within errors with (i) the parameters of  $a_0(980)$  deduced from  $\eta\pi\pi$  data, (ii) the SU(3) prediction for  $g_{KK}^2/g_{\eta\pi}^2$  of  $a_0(1450)$ . However, they do not constrain those parameters well. A close inspection of the  $KK$  mass projection on Fig. 13(d) shows that data favour a slightly narrower  $a_0(980)$  than is fitted. This could arise from either stronger coupling of  $a_0(980)$  to  $KK$  or a steeper form factor, i.e. a larger  $\alpha$  parameter and larger radius of interaction.

A final question is whether there is any significant  $a_0(1450) \rightarrow KK$  signal at all. This may be tested against the fit where  $a_0(1450)$  and  $a_0(980)$  are constrained to their predicted values. To err on the pessimistic side, this test is made including  $\rho(1450) \rightarrow KK$ . Omitting  $a_0(1450)$  from the fit,  $\chi^2$  gets worse by 36.8 with 2 less parameters. This is a change of 5.5 standard deviations, so there does appear to be a signal due to  $a_0(1450) \rightarrow KK$ . The situation is simply that its magnitude cannot be determined with any precision from these data.

## 5.1 Comparison with Kloe data on $\phi \rightarrow \gamma(\eta\pi)$

There are important data from Kloe on this process giving direct and precise information on the line-shape of  $a_0(980)$ . The present status is that data have been published from the first phase of this experiment, with  $\eta$  decaying via both  $\gamma\gamma$  and  $\pi^+\pi^-\pi^0$  [37]. Preliminary results for parameters of  $a_0(980)$  have also been presented from the second stage of this work [38]. A comparison will be made with these preliminary results.

The Kloe data define accurately the  $a_0(980)$  line-shape below the  $KK$  threshold. In the process  $\phi \rightarrow \gamma a_0(980)$ , there is a dependence of the cross-section on  $k_\gamma^3$ , where  $k_\gamma$  is the photon momentum. This factor is the usual  $k^3$  factor for an E1 transition. It inflates the lower side of the  $a_0(980)$  strongly, improving the precision with which it can be measured. However, one must beware that the line-shape may be affected by form factors.

The Kloe group have fitted their data in two ways. The first assumes the  $KK$ -loop model of Achasov and Ivanchenko [39]. In this model,  $\phi$  decays to  $\gamma(KK)$ , then the  $KK$  pair re-scatter via a final state interaction to  $a_0(980)$ , which decays to  $\eta\pi$ . With this model, the preliminary parameters for  $a_0(980)$  are

$$M = 983 \pm 1 \text{ MeV} \quad (21)$$

$$g_{\eta\pi}^2 = 0.156 \pm 0.011 \text{ GeV}^2 \quad (22)$$

$$r_{KK} = \frac{g_{KK}^2}{g_{\eta\pi}^2} = 1.19 \pm 0.05. \quad (23)$$

These values are quite close to those emerging from Crystal Barrel  $\eta\pi\pi$  data, Eqs. (18-20).

The alternative fit made by Kloe ignores the constraint of the  $KK$  loop model and arrives at a value of  $g_{\eta\pi}^2$  seriously different:  $g_{\eta\pi}^2 = 0.096 \pm 0.009 \text{ GeV}^2$ . The agreement between the first set of results and Crystal Barrel data clearly favours the  $KK$ -loop model. The disagreement of the second set illustrates the sensitivity to the precise equations used to fit Kloe data.

The published Kloe data were fitted in earlier work using the  $KK$  loop model [40]. That fit has now been repeated using the parameters for  $a_0(980)$  reported here. There is a significant contribution to the data (up to 18%) from  $\phi \rightarrow \rho\pi$ ,  $\rho \rightarrow \gamma\eta$ . From present publications, it is not clear how much of this contribution is eliminated by experimental cuts. Excellent fits can be obtained with both the Kloe parameters of Eqs. (21-23) and with parameters fitting Crystal Barrel data, Eqs. (18-20) by varying the magnitude and phase of the  $\rho\pi$  combination. The magnitude of the fitted  $a_0(980)$  signal is proportional to  $g_{\eta\pi}^2 g_{KK}^2$  and is constrained to reproduce the latest branching ratios reported in [38]. The fit is almost indistinguishable from that shown in Fig. 3 of [40]. When information from the full Dalitz plot becomes available, the  $\rho\pi$  amplitude can be determined accurately in both magnitude and phase.

## 5.2 Pole parameters of $a_0(980)$

In order to find the pole position of  $a_0(980)$  it is necessary to parametrise the cusp at the  $KK$  threshold in the real part of the amplitude. At the cusp, there is a discontinuity in slope, due to the opening of the  $KK$  channel. If there is no form factor in the  $KK$  channel, this cusp can be calculated algebraically with two subtractions at the  $KK$  threshold. It is given in Ref. [10], Eqs. (8) and (9):

$$\frac{\text{Re } \Pi(s)}{g_{KK}^2} = j_{KK} = \frac{\rho_{KK}}{\pi} \ln \frac{1 - \rho_{KK}}{1 + \rho_{KK}}, \quad s \geq 4m_{KK}^2 \quad (24)$$

$$= -\sqrt{\frac{4m_{KK}^2 - s}{s}} - \frac{2v}{\pi} \tan^{-1} v, \quad s < 4m_{KK}^2, \quad (25)$$

where  $\rho_{KK} = 2k_{KK}/\sqrt{s}$  above the  $KK$  threshold and  $v$  is the modulus of this quantity below threshold;  $k_{KK}$  is the momentum in the  $KK$  rest frame, and is complex below threshold.

With the form factor present, an empirical parametrisation is needed, based on Eqs. (24) and (25). An excellent fit may be obtained to  $\Pi(s)$  from the  $\eta\pi$  threshold to 1.6 GeV replacing these equations by

$$\text{Re } \Pi(s) = f(s) j_{KK} + F_2 + F_3 s + F_8 s_p^2 \quad (26)$$

$$f(s) = \frac{F_1}{1 + F_4 s_r + F_5 s_r^2 + F_7 s_r^3} \quad (27)$$

$$s_r = s - 4m_{KK}^2 \quad (28)$$

$$s_p = s - F_6. \quad (29)$$

Here  $f(s)$  modulates  $j$  with a convergent power series about the  $KK$  threshold. [A similar expression is used for  $a_0(1450)$ ]. The terms  $F_2 + F_3s$  allow for the double subtraction at the  $KK$  threshold. The term  $F_8s_p^2$  is mostly concerned with fitting  $\text{Re } \Pi(s)$  above  $s = 1.5 \text{ GeV}^2$ . Parameters are tabulated in Table 4.

$F_1$	0.722107
$F_2$	0.052635
$F_3$	-0.230099
$F_4$	-0.638335
$F_5$	1.804376
$F_6$	2.165924
$F_7$	1.402098
$F_8$	0.172984

Table 4: Parameters (in units of GeV) fitted to Eqs. (26)–(29).

The physical region lies at  $s + i\epsilon$  for all channels, in the limit  $\epsilon \rightarrow 0$ . The  $\eta\pi$ ,  $KK$  and  $\eta'\pi$  cuts may be labelled by the signs multiplying  $i$  for each channel. The pole closest to the physical region has signs  $+-+$  and lies at  $M - i\Gamma/2 = 989.1 - i40.1 \text{ MeV}$ . It is reached from the physical region by going around the end of the  $KK$  cut and is usually called the second-sheet pole. Tests show that this pole moves little with the  $KK$  form factor. The strong coupling to  $KK$  locks the resonance to the  $KK$  threshold and the full width  $\Gamma = 80.2 \text{ MeV}$  is determined by the fitted value of  $g_{\eta\pi}^2$ . If the sign of  $i$  for the  $\eta'\pi$  channel is reversed, the pole moves to  $997.4 - i46.3 \text{ MeV}$ . The change due to the  $\eta'\pi$  channel is small because the threshold opens at  $1093 \text{ MeV}$  and its coupling is weaker than for  $KK$  and  $\eta\pi$ . However, its effect is not negligible.

Sheet	Pole $M - i\Gamma/2$ (MeV)
$+-+$	$(989.1 \pm 1.0 \pm 3.0) - i(40.1 \pm 1.9 \pm 2.7)$
$---$	$(997.4 \pm 1.0 \pm 5.0) - i(46.3 \pm 1.9 \pm 4.2)$
$+++$	$(920 \pm 3 \pm 20) - i(93 \pm 5 \pm 20)$

Table 5: Pole positions on sheets labelled by signs of  $i$  in channels  $\eta\pi$ ,  $KK$  and  $\eta'\pi$ . The first errors are statistical and the second systematic.

In Table 5, statistical errors are assigned from corresponding errors for fitted values of  $M$  and  $g^2$ . Systematic errors arise from (i) neglect of mass differences between the three  $KK$  charge combinations, (ii) uncertainty about form factors, (iii) isospin mixing with  $f_0(980)$ . The first of these is estimated from half the spread of  $KK$  mass differences. The second is estimated from errors in the exponent of the form factor for the  $KK$  channel:  $\alpha = 2.0 \pm 0.5 \text{ GeV}^{-2}$ . This estimate is obtained from experience in fitting many sets of Crystal Barrel data for wider resonances, where the form factor has a stronger effect. The third error due to isospin violation is unknown at present. However, one expects isospin mixing to produce effects small compared with width differences of  $f_0(980)$  and  $a_0(980)$ ; the second-sheet pole for  $f_0(980)$  has  $\Gamma/2 = 17 \pm 4 \text{ MeV}$  from current BES II data [16]. Systematic effects of the  $\eta'\pi$  channel are hard to estimate without data for that channel. They have been estimated as half the difference between the first and second entries of Table 5.

The position of the pole with  $+++$  signs is further from the physical region than the second-sheet pole. It has changed greatly from earlier fits using Breit-Wigner amplitudes without form factors or Adler zeros. In that earlier work, this pole, commonly called the third-sheet pole, lay close to  $1040 - i83 \text{ MeV}$ . The large change in its mass arises from sensitivity to form factors. In this respect, Crystal Barrel data fitted here, although they determine  $M$  and  $g^2$  with modest errors, do not give accurate information on the precise line-shape in  $\eta\pi$ . This is because of uncertainties in interferences with the  $\pi\pi$  S-wave and open questions about exactly how to parametrise it. Forthcoming Kloe data should improve this situation substantially. The line-shape in those data

measures directly the form factor for coupling of  $\eta\pi$  to the resonance. The systematic error assigned in Table 5 assumes the form factor has exponent  $\alpha = 2.0 \pm 0.5 \text{ GeV}^{-2}$ , corresponding to a Gaussian source with a root mean square radius  $0.68 \pm 0.08 \text{ fm}$ .

Positions of the poles in the sheets  $++-$  and  $+- -$  corresponding to the  $\eta'\pi$  channel will not be given because of the absence of data for that channel.

## 6 Conclusions

Experimental conclusions are straightforward. Firstly, dispersive corrections and the  $s$ -dependence of amplitudes play a major role for both  $a_0(1450)$  and  $a_0(980)$ . The fit to  $\bar{p}p \rightarrow \eta\pi^0\pi^0$  is decisive in settling parameters of  $a_0(1450)$ . Without these data, the width fitted to  $\omega\pi^+\pi^-\pi^0$  data alone is unreasonably small  $\sim 110 \text{ MeV}$ . With the inclusion of decays of  $a_0(1450) \rightarrow a_0(980)\sigma$ , there is an excellent fit to both sets of data, giving the fitted parameters of Table 2. The  $\chi^2$  of both fits improve with the inclusion of the  $s$ -dependence of the  $a_0(1450)$  amplitude. More importantly, the fit stabilises in a narrow range of parameters and the fitted  $a_0(1450)$  signal in  $\eta\pi^0\pi^0$  increases by a factor 1.8; this is a clear indication of a better fit to the line-shape. The overall conclusion is that  $a_0(1450)$  decays weakly to  $\eta\pi$ ,  $KK$  and  $\eta'\pi$  and dominantly to  $\omega\rho$  and  $a_0(980)\sigma$ . It is unfortunate that data on  $\bar{p}p \rightarrow K_L^0 K^\pm \pi^\mp$  do not constrain the ratios  $g_{KK}^2/g_{\eta\pi}^2$  for either  $a_0(1450)$  or  $a_0(980)$  tightly. The data are consistent with the SU(3) predictions.

For  $a_0(980)$ , there is quite good agreement between Crystal Barrel  $\eta\pi^0\pi^0$  data and Kloe data. Each have their merits. A limitation of present data is the mass resolution of Crystal Barrel near the  $KK$  threshold,  $\pm 9.5 \text{ MeV}$ . If progress is to be made on isospin mixing between  $a_0(980)$  and  $f_0(980)$ , a mass resolution better than  $0.5 \text{ MeV}$  seems desirable, i.e. 10% of the spread of  $KK$  masses.

An incidental result is a better understanding of the dominant  $J^{PC} = 0^{-+}$  signal in  $\bar{p}p \rightarrow (\omega\rho)\pi$ . A plausible interpretation of the data is presented in terms of a cusp at the  $\omega\rho$  threshold and a radial recurrence of  $\pi(1300)$  close to  $1730 \text{ MeV}$ . However, more precise data are needed to clarify this result in  $\omega\rho$ ,  $\rho\pi$  and  $[\sigma\pi]_{L=1}$  channels. The Compass experiment could be a good source of such data. Obviously a search for the missing  $a_0$ 's expected at higher mass is sorely needed.

As regards the interpretation of  $a_0(1430)$ , it seems likely to be dominantly an  $n\bar{n}$  state. Black, Fariborz and Schechter have pointed out that  $a_0(980)$  may have a radial excitation in the general mass range of  $a_0(1430)$  [41]. Such a radial excitation would almost inevitably mix with the expected  $n\bar{n}$  state. The radial excitation would respond to long range meson-meson interactions, and therefore to the  $a_0(980)\sigma$  and  $\omega\rho$  thresholds. These are likely to be responsible for pushing the mass of  $a_0(1450)$  up to that of  $K_0(1430)$ .

One of the essential ingredients in fitting all the data is the  $\pi\pi$  S-wave (and  $K\pi$ ). Empirically it is necessary to parametrise it with the 2-component form of Eq. (8). This gives considerably flexibility to the numerator  $N(s)$  of the amplitude, even though the denominator  $D(s)$  is accurately known. Guidance from theory on the way the  $\sigma$  and  $\kappa$  couple in production reactions would be very helpful to experimentalists.

## References

- [1] Particle Data Group, J. Phys. G **33** 1 (2006).
- [2] C. Amsler et al., Phys. Lett. B **333** 277 (1994).
- [3] D.V. Bugg, V.V. Anisovich, A. Sarantsev and B.S. Zou, Phys. Rev. B **50** 4412 (1994).
- [4] C. Amsler et al., Phys. Lett. B **355** 425 (1995).
- [5] A. Abele et al., Nucl.Phys. A **609** 562 (1996); Erratum: Nucl. Phys. A **625** 899 (1997).
- [6] C.A. Baker et al., Phys. Lett. B **353** 140 (2003).
- [7] A. Abele et al., Phys. Rev. D **57** 3860 (1998).
- [8] A. Abele et al., Nucl.Phys. B **404** 179 (1997).
- [9] A.V. Anisovich et al., Nucl. Phys. A **690** 567 (2001).

- [10] D.V. Bugg, J. Phys. G **35** 075005 (2008).
- [11] V. Nikolaenko for the VES collaboration, Meson08 conference, Krakow (June 6-10) 2008.
- [12] D.V. Bugg, Eur. Phys. J C **52** 55 (2007).
- [13] C. Amsler et al., Nucl. Phys. A **720** 357 (2003).
- [14] A. Abele et al., Phys. Lett. B **423** 175 (1998).
- [15] C. Amsler et al., Z. Phys. C **58** 175 (1993).
- [16] M. Ablikim et al., Phys. Lett. B **603** 138 (2004).
- [17] I. Caprini, G. Colangelo and H. Leutwyler, Phys. Rev. Lett. **96** 032001 (2006).
- [18] K.M. Watson, Phys. Rev. **88** 1163 (1952).
- [19] D.V. Bugg, Eur. Phys. J C **54** 73 (2008).
- [20] D.V. Bugg, J. Phys. G **34** 151 (2007).
- [21] Yu. A. Simonov and A.I. Veselov arXiv: hep-ph/ 0804.4635.
- [22] M. Ablikim et al., Phys. Lett. B **607** 243 (2005).
- [23] R. Escribano and J. Nadal, arXiv: hep-ph/0703187.
- [24] C.E. Thomas, JHEP **10** 026 (2007).
- [25] R. Escribano, arXiv: hep-ph/0802.3909.
- [26] A. Abele et al., Eur. Phys. J C **8** 67 (1999).
- [27] A. Bertin et al., (Obelix Collaboration) Phys. Lett. B **434** 180 (1998).
- [28] M. Bargiotti et al., (Obelix Collaboration) Eur. Phys. J C **26** 371 (2003).
- [29] A. Anisovich et al., Phys. Lett. B **485** 341 (2000).
- [30] F. Meyer-Wildhagen, Ph. D. thesis, University of Munich, (2004).
- [31] D.V. Amelin et al. (VES Collaboration), Yad. Fis. **62** 1021 (1999), translated in Phys. At. Nuclei **62** (1999) 445.
- [32] D. Aston et al. (LASS Collaboration), Nucl. Phys. B **296** 493 (1988).
- [33] D.V. Bugg, Phys. Lett. B **632** 471 (2006).
- [34] D.V. Bugg, Eur. Phys. J A **25** 107 (2005).
- [35] E.M. Aitala et al. (E791 Collaboration), Phys. Rev. D **73** 032004 (2006).
- [36] B. Aubert et al. (Babar Collaboration), arXiv: hep-ex/0710.4451.
- [37] A. Aloisio et al. (Kloe Collaboration), Phys. Lett. B **536** 209 (2002).
- [38] F. Ambrosino et al. (Kloe Collaboration), arXiv: hep-ex/0707.4609 (2007).
- [39] N.N. Achasov and V.N. Ivanchenko, Nucl. Phys. B **315** 465 (1989).
- [40] D.V. Bugg, Eur. Phys. J C **47** 45 (2000).
- [41] D. Black, A.H. Fariborz and J. Schechter, Phys. Rev. D **61** 074001 (2000).